

AD-A059 700

PROPELLANTS EXPLOSIVES AND ROCKET MOTOR ESTABLISHMENT--ETC F/G 21/8
CURRENT TECHNIQUES FOR THRUST MEASUREMENT AT PERME WESTCOTT.(U)

FEB 78 D S DEAN

UNCLASSIFIED

PERME-TR-50

DRIC-BR-61445

NL

1 OF 1
AD
A069700



9700

PERME TR 50

UNLIMITED
LEVEL

(18) DRI C

(19) BR61445

AD A059700



PROCUREMENT EXECUTIVE
MINISTRY OF DEFENCE

**Propellants, Explosives
and Rocket Motor
Establishment,
Westcott, Aylesbury, Bucks**

DDC FILE COPY

(9) **Technical Report 50**

DDC
OCT 10 1978

(6) **Current Techniques for Thrust
Measurement at PERME Westcott.**

(10) D. S. Dean

(11) February 1978

(12) 99p.

78 09 28 018
410411
UNLIMITED

PROPELLANTS, EXPLOSIVES AND ROCKET MOTOR ESTABLISHMENT
WESTCOTT

Technical Report No. 50

Approved September 1977

CURRENT TECHNIQUES FOR THRUST MEASUREMENT AT PERME WESTCOTT

by

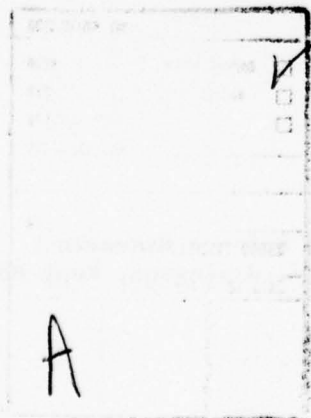
D.S. Dean

SUMMARY

Techniques are described for the accurate measurement of axial thrust and thrust alignment of rocket motors, although the principles are applicable to force measurement in any other field. The dynamic response of systems is considered and techniques are described by which this may be adapted to give a linear characteristic to well above the natural frequency of the rig. This includes both amplitude and phase response.

For simpler systems a method of evaluating and predicting response to linear ramp functions is derived.

A ballistic technique for recording total impulse and the thrust/time curves of motors with very short burning times, which avoids most of the problems associated with the use of ballistic pendula is described. The principles are applicable to the measurement of other quantities in addition to thrust.



78 09 28 018

Copyright



Controller HMSO London
1978

Further copies of this report can be obtained from the Defence Research
Information Centre, Station Square House, St. Mary Cray, Orpington, Kent BR5 3RE.

CONTENTS

	Page
1 INTRODUCTION	5
2 GENERAL PHILOSOPHY OF DESIGN	5
3 SIMPLE AXIAL MEASUREMENT OF FORCE	6
3.1 General arrangement	6
3.2 Damper units	8
3.3 Pipe connections	9
3.4 PERME load cell	9
4 MEASUREMENT OF THRUST ALIGNMENT	11
4.1 Determination of vertical thrust alignment	11
4.1.1 The general problem	11
4.1.2 Design of firing bay	11
4.1.3 Design of thrust stand	12
4.1.4 Alignment and calibration	13
4.1.5 Recording and analysis	15
4.1.6 Conventions used in analysis	17
4.1.7 Accuracy	18
4.2 Determination of horizontal thrust alignment	18
4.2.1 Additional problems with horizontal firings	18
4.2.2 Design of thrust stand	19
4.2.3 Computer corrections	19
4.2.4 Calibration	20
4.2.5 Static test of rig	21
4.2.6 Accuracy	22
4.3 System with dual thrust axes	22
4.3.1 Discussion of problems with dual thrust axes	22
4.3.2 Design of stand	23
4.3.3 Calibration	23
4.3.4 Impulsive loading	23
4.3.5 Assessment of accuracy	24
5 MEASUREMENT OF TRANSIENT FORCES	26
5.1 Theoretical discussion	26
5.2 Complete evaluation of equation of motion	28

ACCESSION FOR	
WIS	Wire Section
DDC	B.H. Section
UNANNOUNCED	
JUSTIFICATION	
BY	
DISTRIBUTION/AVAILABILITY CODES	
2-1	SPECIAL

	Page
5.2.1 Practical rig construction and signal conditioning	28
5.2.2 Calibration	29
5.2.3 Practical problems and results	29
5.3 Ballistic measurement of impulse and thrust	30
5.3.1 Basis of the ballistic approach	30
5.3.2 Ballistic measuring systems	30
5.3.3 Description of system	32
5.3.4 System accuracy	33
5.3.5 Use of the equipment	34
5.3.6 Summary of advantages	35
5.4 Transient behaviour of system measuring only displacement	35
5.4.1 Discussion of rig response	35
5.4.2 Mathematical solution	36
5.4.3 Determination of damping ratio	40
5.4.4 Use of electrical analogue	41
5.4.5 Results	42
6 CONCLUSIONS	43
7 REFERENCE	44
Appendix 1 Stiffness of flexure units	45
Appendix 2 Damping force generated by axially moving piston	48
Appendix 3 Effects of strut misalignment	50
Appendix 4 Analysis of data from thrust alignment records	53
Appendix 5 Design of hydraulic clamp	57
Appendix 6 Analysis of ballistic pendulum	58
Appendix 7 Decelerating device (initial design)	61
Appendix 8 Examples of the use of graphs giving dynamic response	63
Tables 1 to 3	66-68
Illustrations - Figs 1 to 37	

1 INTRODUCTION

Over the past decade thrust measurement techniques at PERME Westcott have been steadily improved and individual systems have been described in reports and memoranda. It was thought desirable, and more convenient for the reader, to gather together this information and descriptions of newer systems in one publication, taking the opportunity to bring the older publications up to date and to include experience of the use of the systems described. There are many relatively minor design features which can have a marked effect upon the accuracy of the overall system. Although these often seem obvious when pointed out, they are frequently overlooked by those unfamiliar with rig design. Because of the possible pitfalls, rig design has tended to be undertaken by a small specialist group at the Establishment but it is hoped that this report will enable any competent engineer to avoid these pitfalls.

As maximum thrust may be attained in only a few milliseconds, the transient response of measuring systems is vitally important and conventional techniques have proved to be inadequate in this respect. Much remains to be done in this particular context and many of the solutions may lie with computer based signal conditioning. Modern data collection and reduction systems are capable of meeting this need and it is becoming progressively more cost effective to use dedicated micro-computers.

A further object is to provide rig designers and site operators with information and solutions to problems in a form, often graphical, which can be used easily. In the writer's experience, it is necessary when analysing rig behaviour to refer to a number of theoretical sources which are often in a form not easily applied to the problem in hand. It is hoped that this report will ease this difficulty.

2 GENERAL PHILOSOPHY OF DESIGN

A rocket motor whose performance is to be determined must be supported while the force which it generates is measured. The supports must not resist the motion of the motor against the measuring device, so that rollers and bearings are generally unsuitable. Even if their coefficients of friction can be kept within acceptable bounds when they are in perfect adjustment, they may deteriorate rapidly under firing site conditions. Flexure devices generally offer the best, cheapest and most robust form of support.

In most cases the measuring system should be as stiff as possible to raise the natural frequency of the rig above any of the Fourier components of the

thrust/time curve. One of the most satisfactory transducers which meets this need is a strain gauge load cell which must be mounted on a stiff thrust block in such a way as to prevent side loads from being applied to the cell. The weight of the moving part of the rig should be kept to a minimum consistent with stiffness.

Because reduction of friction increases the magnification factor, Q , of the rig (see page 27), some form of damping, involving no static friction, may be required. Electrical filtering of the signal may be possible, but lack of mechanical damping results in large oscillatory forces in the rig which may cause damage.

Calibration of the measuring cells should be possible without their removal from the rig so that any restriction of movement by the rig is taken into account. This has the advantage that any deterioration in the performance of the rig is noticed during calibration.

A horizontal thrust line is preferred if axial thrust only is to be measured, so that change of weight during burning does not appear in the thrust measurement. If thrust alignment is to be measured, however, the thrust axis should be vertical, so that change of weight does not affect the small side forces but affects only the much larger axial force.

When firing times are less than about 10 ms it is often impossible to raise the natural frequency of the rig sufficiently and it may then be best to use a system having zero stiffness and to measure thrust by the acceleration of the motor and a suitable mass. An accurate measure of total impulse can then be obtained from the momentum of the mass. An alternative technique is to measure the applied force by vector addition of the acceleration, displacement and damping of the rig.

Typical applications of these principles are given in the following descriptions of firing rigs in use at PERME Westcott.

3 SIMPLE AXIAL MEASUREMENT OF FORCE

3.1 General arrangement

Fig. 1 represents a typical flexure stand for use when only axial thrust is to be measured. The motor is clamped into support frames hanging from plate flexures which allow it to move with minimal restriction in the axial direction. Thrust is measured by a combined load cell and damper unit coupled to the motor forward head by a flexure unit permitting slight axial misalignment which would

otherwise generate large lateral forces in the rig. The support flexures must be allowed to hang vertically or the effect of gravity on the motor mass (M) would generate an axial force of $M \tan \theta$, where θ is the inclination of the flexure which, for small angles, is given by $\tan \theta \approx x/h$, where x is the displacement of one end of the flexure relative to the other end and h is the length of the flexure. This in itself does not cause an error, but when the motor mass changes during firing this force changes, resulting in a progressively increasing error and a zero shift at the end of the firing. Target accuracy in our thrust measurements is 0.1% so that if M_c is the charge mass and T the motor thrust

$$M_c \tan \theta \leq 10^{-3} T$$

or

$$\frac{x}{h} \leq \frac{10^{-3} T}{M_c}.$$

The longer the flexure the greater the displacement error that can be tolerated. For a typical boost motor of 25000 N thrust and 50 kg mass $\tan \theta$ is 0.05, which is easy to achieve, but for sustainer motors of low thrust/mass ratio permissible errors are small.

A further source of error may be the expansion of the motor due to internal pressurisation during firing which can typically be 2.5 mm in a motor 3 m long. This inclines the flexures and generates a bending force in them along the motor axis. To prevent this the motor support frames should be coupled to the alignment flexure as shown in Fig. 1. This implies that the motor must slide in its clamps and that their tension should be suitably adjusted. For large motors secondary flexures may be required to permit this expansion.

Calibration of the rig is usually carried out using a Macklow-Smith capsule as a ram and a standard load cell, accurate to $\pm 0.05\%$, to measure the force. This may be applied via a compression rod in place of the motor or by tie rods from the rear of the thrust block. The Macklow-Smith capsule consists of a low aspect ratio piston and cylinder with the piston located and bonded to the cylinder by a rubber seal.

The load cell is compensated for temperature effects, but the moduli of the support flexures change with temperature and should therefore represent as small a proportion as possible of the total restoring force. It is desirable to keep their stiffness to less than 0.1% of that of the load cell and coupling devices.

This is not always possible and in such cases in situ calibration is necessary at the temperature at which the firing will take place.

Flat plate flexures present minimal resistance to bending imposed by axial motor movement, but are stiff in all other directions. An analysis of flexure design is given in Appendix 1. A simple flat plate of constant thickness acts as a flexure and assumes an S bend as in Fig. 1 if it is used in a rig such as that just described. Since bending is zero in the middle of the flexure and a maximum at the roots the stiffness is altered only slightly by thickening the flexure in the middle and allowing bending only over two short lengths at each end. This has the advantage of considerably raising the crippling load under which the flexure will fail in compression. The flexures may, of course, be mounted in compression provided that this crippling load is not exceeded. To resist crippling by a greater margin a more complicated flexure, which has two subsidiary flexures to maintain the alignment of the main flexure blade, is sometimes used (see Fig. 2). If parts of the flexure are bolted together, or if the flexure as a whole is bolted to its supports, these bolted parts must be stiff enough to prevent relative movement, which would appear as hysteresis in the measurements. If the flexure stiffness is kept below 0.1% of that of the measuring system these effects are negligible. The alignment flexure between motor and load cell is similar in principle to the support flexures but is of circular section instead of flat plate because movement in any direction may be required.

3.2 Damper units

Many designs of damper unit have been used and the latest is shown diagrammatically in Fig. 3 and in detail in Fig. 9. All generate damping forces by pumping oil from one side to the other of a piston through an annular gap. There are no contacting surfaces so that static friction is eliminated. The main coupling rod and its piston are supported with correct clearance in the cylinder by diaphragms, which also retain the damping oil. The clearance around the rod at each side of the piston is less than that around the piston to minimise the amount of oil escaping into the reservoirs, sealed by the diaphragms. Quick release couplings at each end of the coupling rod attach it to the alignment flexure and to the load cell. The damper is mounted on the front of a cylindrical housing which contains the load cell. All load cells are adjusted to be the same length so that they can be interchanged without disturbing rig alignment. As movements to be damped are usually less than 0.1 mm the damper support must be very rigid or it would act as a spring rather than a damper. An analysis of the damper operation in the form of a simple piston and cylinder is given in Appendix 2.

To achieve sufficient stiffness the thrust block should be much stronger than is required merely to resist the maximum thrust, and any metal structure should be embedded in concrete to reduce parasitic oscillations which might appear in the thrust recording.

3.3 Pipe connections

When pipe connections to the rig are required, such as with liquid propellant rocket engines, the greatest care must be taken to prevent them from applying varying loads to the rig. A constant load is generally acceptable as this is automatically ignored by the calibration and signal analysis systems. Flexible piping is unsuitable as it exerts considerable forces when pressurised; the aim should be to use piping which acts elastically in bending, its stiffness in this condition usually being much less than that of the measuring system. The pipe should be led in at right angles to the rig axis and may even form one of the motor flexural supports. When forces are to be measured in other directions as well as that of the rig axis, the pipe must be flexible in more than one direction and an arrangement such as that shown in Fig. 4 is required. Here all sections of the piping which are required to flex are straight and all changes of direction are made within a stiff block which does not deflect appreciably under pressure. This arrangement allows movement at the motor end in any direction with little resistance to motion, and deflection due to internal pressure in the pipe is minimised. A coil in the pipe is inadmissible as this generates forces when the pipe internal pressure changes. To prevent hysteresis effects anchorage of the pipe at each end should be such that no movement is possible. If the stiff blocks in which changes of direction of the pipes are made are heavy they may vibrate on the pipes and this vibration may appear in the thrust record. To avoid this a simple flexure support at the block may be used. When small side forces are to be measured the pipes should be blanked off at the motor end and pressurised to evaluate any small resultant forces.

3.4 PERME load cell

For many purposes selected commercial load cells are adequate, but a cell designed at PERME Westcott is used when there is a possibility of an overload damaging the commercial cell. The design was originally described in 1960, but modern manufacturing techniques have enabled its performance to be improved and its overload capability is still unsurpassed.

Its construction is shown in Fig. 5 and it consists of an inner and outer ring of strain gauged struts, each ring usually consisting of eight struts. The

load is applied to a central pillar so that the inner ring is in tension. The upper ends of the inner struts are coupled to those of the outer struts, which are in compression, as their lower ends are coupled to the base of the load cell. The member to which the central pillar is connected is separated from the base by a gap of about 0.07 mm, which can be adjusted by shims between the bottom of the outer ring and the cell base.

When a load is applied to the central pillar the gap closes when the strain in the struts is about 0.15% and the stiffness of the structure then increases by at least 20:1, so that an overload of this magnitude can be tolerated before the acceptable strain on the struts is exceeded. The overload range of the cell can be increased by using thinner shims at the expense of a lower working range. Each strut has a strain gauge on either side of it, measuring the axial strain, making 32 gauges in all. These are usually coupled in groups of 16 to form two Wheatstone bridges with all arms active. Alternate struts form the elements of one bridge to distribute strain evenly between the bridges in the case of non-axial loading of the cell. Two gauges per strut are employed to cancel any effects of bending.

The earlier designs of cell incorporated two concentric rings coupled by flanges at their upper ends, which could give rise to hysteresis caused by slight relative movement. The latest design is formed from one piece of material, the gap between the rings of struts being formed by spark erosion. This allows the gap to be reduced to about 2 mm with a consequent reduction in bending moment at the coupling flange and elimination of the bolted joint. The material used is EN30B air hardening steel, which exhibits very low hysteresis. The upper end of the central pillar is supported by a diaphragm to reduce lateral loads on the measuring struts.

To measure widely differing loads in the same rig the smaller cell may be fitted in place of the central pillar of the larger cell. During the high load period the smaller cell bottoms and continues to record at a lower sensitivity. The output of the larger cell is then more accurate as that from the smaller cell is affected slightly by the manner in which the cell bottoms. If an accuracy of about $\pm 3\%$ is adequate the output of the smaller cell in the bottomed condition may be used. Under normal conditions the cells can achieve a repeatability of 0.05%.

4 MEASUREMENT OF THRUST ALIGNMENT

4.1 Determination of vertical thrust alignment

4.1.1 The general problem

For many missile applications it is important to know the deviation of the line of action of the thrust vector from the geometric axis of the motor. This permitted deviation may be as small as 0.5 mrad, so that measured accuracy must aim at resolving at least to 0.1 mrad.

Consider a motor of 5000 N thrust; the maximum permitted side force is about 2.5 N and the measuring accuracy must be ± 0.5 N. Greater accuracy would be desirable, but cannot be achieved with current systems as measurement of such small side forces in the presence of a large axial force is difficult. It becomes more difficult when the axial force is applied in a period which may vary from 2 to 10 ms and fluctuates rapidly during the firing, which may occupy less than a second. In addition, the direction of the thrust vector usually fluctuates rapidly during firing.

Although stiffness is highly desirable, as in the simpler rigs, coupling between cells measuring forces in different directions must also be reduced. This involves flexures which increase displacement along the cell axes and hence reduce stiffness. The design philosophy adopted at PERME is to reduce coupling to such a low value that only interaction in the side cells due to axial force need be considered. This results in rig natural frequencies of about 100 Hz.

4.1.2 Design of firing bay

To deal with rapid changes in thrust alignment it is necessary to raise the natural frequency of the complete system, including rig and supporting structure, above any components of the thrust transient which are to be measured. During a firing alignment of the rig must be maintained to within about 0.05 mm. Although some elastic displacement takes place in the rig it is thus still necessary to construct a stiff and massive structure to support the rig. A bay, made of reinforced concrete and capable of sustaining much higher loads than would be imposed by a rocket motor, was built in the form shown in Fig. 6. Axial thrust is taken on a plate let into the floor and side thrust on the two concrete buttresses to which the side struts can be attached at various levels as required. The flat plates to which the side struts are attached are bolted to a rigid frame and Araldite was poured between the plates and the frame to prevent flexing (see Fig. 7). This has the added advantage of damping the plates.

4.1.3 Design of thrust stand

The rig (Fig. 7) was originally constructed within a steel frame which mated with the fixed members in the bay so that the complete unit could be lifted out and replaced as required. This proved to be a mistake because the frame had always to be re-aligned in the bay after replacement and the necessary adjusters introduced flexibility which increased strut interaction. A modification was introduced whereby the axial thrust member was attached rigidly to the plate set in the bay floor and was unconnected with the side member frame. This eliminated transient interaction effects at motor ignition which had previously been troublesome.

The motor is held in a sub-frame which must be as rigid and as light as possible and must have accurately machined surfaces to mate with the datum surfaces on the motor which define its geometric axis. This frame is supported by six struts, d , e and h being orthogonal, f and i being parallel to e and h respectively and g being parallel to e but displaced by a distance c' in the plane of e and h . The motor thrusts vertically downwards in line with strut d and side forces are measured in one plane by f and e and in the other at right angles by i and h . g could be used to measure the torque forces but is not instrumented for reasons discussed later. The motor is fired vertically so that the change of charge weight during firing is solely a component of the axial thrust. Any asymmetry in burning about the vertical axis results in forces in the side struts which cannot be distinguished from those due to thrust alignment, but this effect is usually small. The computer correction described in Section 4.2.3 can be used to correct for this on the assumption that movement of the centre of gravity is linear with respect to propellant consumption.

Ideally, each strut should have a frictionless universal joint at each end so that it can resist only forces along its axis, the measuring load cell being mounted between these joints. In practice, to minimise friction, the cell is mounted between short rod flexures which, although stiff in compression, permit sideways movement of the strut end under a small reproducible force which can be calibrated out of the system. In strut g the cell is omitted and the flexures are connected by a solid bar. The construction of a strut is shown in Fig. 8.

The virtual elimination of friction implies that any oscillation induced by motor transients, particularly on ignition, persists as a decaying oscillation long after the initial disturbance has ceased. Oscillatory drive forces near the natural frequency result in such high oscillatory forces in the side struts that

analysis is impossible and the load cells may be destroyed. To overcome this difficulty hydraulic dampers, similar to those described in Section 3.2, are mounted at the motor ends of all the struts. If the correct grade of oil is used it is possible to damp the structure critically. The oil is retained by metal flexible seals secured by Araldite. This early damping device, although otherwise satisfactory, proved difficult to align and will be replaced eventually by the later design shown in Fig. 9. A theoretical treatment of these dampers is given in Appendix 2.

4.1.4 Alignment and calibration

The ends of the thrust struts are clamped to the fixed parts of the damper to permit initial alignment of the rig, and the clamps are removed before final alignment. Unfortunately any strain in the flexures is relieved, resulting in the damper parts becoming eccentric or even binding. To detect this a guide similar to the clamp is used, with a small clearance on one member of the damper, which is checked with a feeler gauge to ensure that the gap is constant at all points. The initial rig alignment is accomplished by using an analogue of the motor body, which reproduces all the datum surfaces of the motor and provides a plane surface, at a convenient height, normal to the geometric axis of the motor. Thus, when this plane surface is set level, by adjusting the lengths of the struts, the geometric axis is set vertical. With a good commercial spirit-level the error need not exceed 0.05 mrad. At this stage the axial strut is assumed to be truly vertical and the side struts are aligned by careful measurement. The criteria for accuracy of alignment of these struts are given in Appendix 3 but the axial strut must be aligned so that the axes of the upper and lower flexures are within 0.03 mm (0.0012 inch) of the motor axis. The upper flexure is positioned to within these limits by accurate machining of all fittings and the lower end of the strut is adjustable by screws in the planes of the side struts. Adjustment is made by applying a known vertical load along the axis of the rig and altering the position of the lower end of the main strut and the length of the side struts until the side loads are within acceptable limits. These residual side loads are applied as corrections to the measured side loads obtained during a firing.

The problem of applying a vertical load accurately was solved initially by machining a frame which fitted the datum surfaces on the rig and suspending weights, by a steel wire, from an accurately located point on the frame. This is still the most accurate method for low thrusts. The maximum force which could be applied by this device was about 1300 N (300 lbf) and it was necessary to

extrapolate linearly the interaction figures for motors generating a higher thrust. This has been superseded by the application of a vertical load through a long strut consisting of a hollow tube with a flexure at each end. This is aligned vertically on the motor axis and a force applied to its upper end (Fig. 10).

The diameters of the flexures of this strut are as small as possible consistent with sustaining the compressive load, and the force may therefore be considered to act along their axes. The strut is about 2.5 m (100 inches) long and is aligned by means of a plumb line suspended inside the tube, from a hole drilled on the centre line of the upper flexure, with the plumb bob hanging between four contacts mounted on the lower flexure. The contacts are adjusted by means of a mandrel to be concentric with the axis of the lower flexure, and their surfaces lie on a circle 0.1 mm (0.004 inch) greater in radius than the plumb bob. The plumb line is conductive and is connected electrically to the tube, whilst the contacts are insulated and each is connected to its own bulb and to a battery in a small portable box. When the strut is vertical the plumb bob does not touch any contact and all lights are out. Any light which is on indicates the direction in which the strut is inclined. With all lights out the bob is less than 0.1 mm (0.004 inch) from the axis and hence the angular misalignment cannot be greater than 0.04 mrad. The plumb line is undisturbed by wind and the accuracy is not affected by any distortion of the tube, as location is governed by the end flexure fittings. The end fittings can be changed to allow for different thrust ranges and different motor attachment points; fluid damping has been allowed for, but found unnecessary.

The lower end of the strut is clamped to the rig by a quick release coupling with accurate location and the upper end fits similarly to a solid rod with a standard load cell fitted to its upper end. As the strut is clamped in place, any small moments introduced by slight bending of the flexures remain constant during calibration and can therefore be ignored. The rod is constrained to move with a parallel vertical motion by two pairs of flexures mounted on the bay wall, and the weight of the complete assembly is just balanced by low rate springs attached to overhead rigid beams (Fig. 10). Between these beams and the solid rod, and attached to the beams, is a Macklow-Smith capsule with a small gap between its piston and the standard load cell. When the capsule is pressurised it acts as a ram and applies controlled loads to the load cell and rod system. The magnitude of the load can be measured to better than 0.1% by the standard load cell and a digital voltmeter. As the movement of the solid rod is

constrained to be vertical it can neither exert side loads on the main rod nor apply bending loads to the upper flexure. The flexures controlling the solid rod are attached to it by screwed ends and knurled clamping nuts, so that it can be moved sideways in two planes to set the main strut in a vertical position. Once the solid strut has been aligned vertically the knurled nuts must always be adjusted in pairs to retain this verticality. Before a firing the calibration strut is removed and the remaining structures swung to the sides of the bay.

To calibrate the lateral struts, weights are added to a pan suspended from a light string which passes over low friction pulleys and is attached to fixtures in line with each of the lateral struts.

4.1.5 Recording and analysis

For most firings on this rig a digital recording system with a sampling rate of 1 kHz has been used. This is multiplexed into 10 channels of which 5 are used to record the load cell outputs. A sample and hold unit ensures that all cells are sampled coincidentally, although subsequent digitisation is carried out sequentially. High sampling rates are now possible using transient recorders, but these limit the duration of firing at any selected sampling rate. A replacement digital recording system which is nearing completion will permit an overall sampling rate of 40 kHz.

To prevent overloading of the side channels due to forces generated by vibration 40 Hz filters are inserted before the amplifiers and a 200 Hz filter in the axial channel. The resultant vibratory forces can be further averaged, if required, but the initial filtering is necessary as the average would not be correct if any overloading occurred during peak loads. The computer can be programmed to average over any selected period, a reasonable lower limit being 50 ms. It corrects each side load reading for the previously determined, residual interaction effects by reference to the axial thrust at that time and calculates results from the analysis given in Appendix 4. The final print-out is in the form of the example which follows.

TIME	THRUST	LOWER		UPPER		ALPHA	BETA	L	N	ERROR IN NOZZLE PLANE	
		RIGHT	LEFT	LEFT	RIGHT					LENGTH	ANGLE
0.03	332.6	1.083	1.550	-1.838	4.638	0.9856	-0.0457	937.42	7526.19	7.1148	36.77
0.06	641.6	0.284	0.646	-2.935	5.175	0.5769	-0.2045	1129.00	1514.13	1.4011	41.93
0.13	683.2	0.001	0.418	-1.147	5.431	0.4555	-0.0611	180.84	1858.13	0.7537	25.73
0.18	722.7	-0.953	-0.407	-1.356	6.263	0.4210	-0.1193	1392.85	1054.43	1.2975	-104.85
0.23	757.1	-1.390	-0.407	1.772	5.448	0.3071	0.1033	1585.40	1533.41	2.0273	-106.06
0.28	781.7	-1.352	-0.366	0.039	5.581	0.3100	-0.0240	1558.56	-141.13	1.9081	-107.41
0.33	810.3	-0.800	-0.487	0.802	5.918	0.3619	0.0081	1365.66	6196.54	1.1486	-127.82
0.38	839.2	-0.450	-0.509	1.014	6.311	0.4001	0.0345	1271.78	2372.67	0.7745	-153.33
0.43	866.4	-0.520	-0.162	2.616	5.485	0.3945	0.1623	1284.02	1259.09	0.4397	-103.82
0.48	898.4	-0.269	0.184	2.609	7.234	0.4442	0.1781	1226.62	1103.06	0.3715	-5.33
0.53	932.5	-0.125	0.752	3.736	7.969	0.4820	0.2758	1199.75	983.02	1.1653	9.24
0.58	959.0	-0.274	0.768	3.624	8.258	0.4770	0.2624	1221.58	974.50	1.1330	0.18
0.63	989.9	-0.532	0.967	3.500	9.075	0.4345	0.2586	1254.59	925.42	1.3676	-11.87
0.68	1016.9	-0.314	1.013	4.744	9.505	0.5179	0.3244	1221.37	973.16	1.4089	0.23
0.73	1043.7	-0.839	0.682	5.184	9.855	0.4950	0.3220	1290.88	1043.67	1.1656	-30.70
0.78	1074.5	-0.810	0.351	5.444	10.186	0.5000	0.3090	1283.03	1109.44	0.8075	-41.26
0.83	1107.3	-0.759	0.378	5.380	10.362	0.4338	0.2979	1274.98	1103.51	0.7668	-36.54
0.88	1138.6	-0.780	0.453	6.479	10.647	0.4566	0.3489	1274.33	1114.67	0.8508	-32.21
0.93	1167.1	-0.879	0.234	3.933	10.850	0.4895	0.2046	1285.09	1114.67	0.6613	-54.59
0.98	1197.6	-1.084	-0.491	6.089	11.329	0.4902	0.2679	1305.91	1284.48	0.7750	-112.14
1.03	1231.9	-0.536	0.226	7.055	11.407	0.5057	0.3387	1239.19	1144.37	0.4623	-18.30
1.08	1270.2	-1.363	-0.745	4.822	11.590	0.4582	0.1839	1339.52	1396.81	1.0944	-120.84
1.13	1296.1	-1.055	-0.595	6.616	11.657	0.4687	0.2662	1298.53	1297.80	0.7182	-119.36
1.18	1325.5	-1.494	-1.122	7.612	11.942	0.4516	0.2805	1349.85	1385.28	1.2883	-128.42
1.23	1355.5	-1.214	-0.666	6.730	11.693	0.4430	0.2564	1317.81	1310.60	0.8401	-118.16
1.28	1393.2	-1.492	-0.479	9.091	11.857	0.4263	0.3542	1350.95	1246.66	0.9714	-99.03
1.33	1424.1	-1.876	-1.742	10.272	12.040	0.4089	0.3432	1399.02	1422.26	1.7421	-133.51
1.38	1449.4	-1.260	-0.574	8.878	12.191	0.4321	0.3283	1317.16	1262.61	0.7544	-107.96
1.43	1478.3	-0.883	-0.240	12.193	12.610	0.4545	0.4633	1269.92	1204.71	0.4050	-69.81
1.48	1496.8	-0.919	0.625	9.695	12.884	0.4580	0.3950	1271.70	1109.50	0.8714	-27.13
1.53	1520.0	-0.380	0.906	13.431	13.004	0.4759	0.5404	1216.52	1106.40	1.0912	2.39
1.58	1547.3	-0.163	1.732	14.909	13.688	0.5007	0.6161	1195.25	1058.09	1.7777	7.56
1.63	1571.8	-0.275	0.362	16.645	14.066	0.5027	0.6200	1204.57	1155.85	0.7319	12.06
1.68	1589.8	-0.874	0.753	16.384	14.641	0.4962	0.6177	1255.96	1129.10	1.0437	-16.37
1.73	1501.0	-1.205	0.397	16.458	14.313	0.5004	0.6435	1289.57	1153.15	0.9726	-37.35
1.78	1342.7	-1.335	-1.405	15.532	13.464	0.5176	0.6029	1311.03	1298.43	1.1373	-135.00
1.83	1161.6	-1.397	-1.513	14.934	12.647	0.5550	0.6621	1327.61	1314.12	1.4761	-136.14
1.88	1021.2	-1.252	-1.052	11.504	11.676	0.5849	0.5865	1322.83	1299.89	1.3019	-127.76
1.93	962.4	-1.440	-0.871	10.818	11.130	0.5769	0.5922	1356.48	1284.41	1.4997	-115.47
1.98	791.6	-1.679	-3.552	10.382	9.775	0.5861	0.4945	1425.97	1795.03	5.3671	-157.13
2.03	614.5	-1.554	-2.203	10.327	8.299	0.6291	0.7577	1453.03	1501.27	4.4797	-145.52
2.08	470.8	-1.663	-0.975	8.318	6.601	0.6011	0.9546	1578.67	1327.84	4.1355	-115.23
2.13	332.6	-1.152	-0.875	5.230	4.482	0.7503	0.7503	1589.45	1418.23	4.4875	-124.93
2.18	172.9	-0.059	-0.480	1.559	2.300	0.7430	0.3574	1211.86	1707.35	3.0299	177.51
2.23	46.9	0.276	0.111	1.503	-0.001	-0.8863	1.9740	1631.26	1100.03	7.5931	56.42
2.28	0.6	0.443	0.776	-0.839	0.019	-60.1918	8.2194	48.44	15703.24	1657.4558	30.69

The error angle is defined by being zero, when error is in direction of the left pair of struts and being 90 degrees when error is in direction of right pair.

The distance between the two pairs of struts is 1181.00

The distance from the lower pair to the centre of gravity is -1222.00

The first column of the results represents the mid-point (rounded up to the nearest 10 ms) of the interval over which all results have been averaged, timing starting at the ignition pulse. The second column is axial thrust in lbf.

The following four columns are side forces in lbf:

- right lower side strut is No. 1;
- left lower side strut is No. 2;
- left upper side strut is No. 3;
- right upper side strut is No. 4.

α is the angle, in degrees, between the vertical and the projection of the thrust vector on the plane in which the axes of the right hand struts lie. β is the angle, in degrees, between the vertical and the projection of the thrust vector on the plane in which the axes of the left hand struts lie. L is the vertical height, in mm, from the origin to the point where the thrust vector intersects the plane in which the axes of the left hand struts lie. M is the vertical height, in mm, from the origin to the point where the thrust vector intersects the plane in which the axes of the right hand struts lie. Error length is the distance, in mm, from the main axis to the point at which the thrust vector passes through a selected horizontal plane, in this case the nozzle plane, 1222 mm above the origin.

The error angle is the angle, looking vertically downwards, between the left hand struts and a line connecting the rig axis to the point where the thrust vector passes through the error plane.

4.1.6 Conventions used in analysis

The planes in which measurements are made are shown in Fig. 11. The origin is taken as the point of intersection of the axes of the two lower struts and the main axial strut. The conventions for the sign of the thrust measurements are such that measurements in the same sense as the calibration loads are considered positive.

Conventions are as follows.

Axial thrust Compression loads are positive

Side thrusts Tension loads are positive

Angles α and β are positive when the resolved part of the thrust vector parallel to the side struts results in a mean tensile force in those struts.

Distances L and M and from origin to the error plane are positive when measured upwards from the origin.

Error length is always positive.

Nozzle angles are measured from zero in the direction of the left pair of struts through 90° in the direction of the right pair of struts to 180° . Angles from 0° to 180° in the opposite direction are negative. The programme has since been modified so that the negative angles are replaced by a continuous rotation from 180° to 360° .

4.1.7 Accuracy

The load cells in use are of American "Bytrex" manufacture embodying semiconductor strain gauges, and are capable of an accuracy of 0.1% of calibrated range. It is necessary to use higher range cells in the side struts than the measured forces indicate, to prevent vibratory damage and damage due to accidental blows on the rig. However, the accuracy of the cells is maintained down to 10%, or less, of their maximum range. It must also be appreciated that an error of up to 10% in side force measurement would be within the limits imposed by alignment errors in the rig and the motor structure when misalignments of about 1 mrad are to be measured. When motors weighing more than about 10 kg are loaded a controlled loading device must be used to avoid impact damage to the load cells. This allows the last few millimetres of motor movement to be controlled by screw adjusters after the motor is fitted to the handling rig.

To check the validity of the assumption that axial thrust acts through the centre line of the calibration thrust rod flexures, this was rotated through 180° and axial thrust steps again applied. The greatest variation between readings in the two positions was 0.08 kg corresponding to a misalignment error of less than 0.1 mrad. Typical interactions obtained in a test are shown in Table 1.

Accuracy during firing can only be estimated, because accurately applied dynamic loads cannot be obtained, but it seems reasonable to expect that the thrust vector can be determined to ± 0.25 mrad.

4.2 Determination of horizontal thrust alignment

4.2.1 Additional problems with horizontal firings

It is always preferable to make thrust alignment measurements with the intended axial line of thrust vertical. This ensures that any change of weight appears as an error in the axial thrust only when it forms a small part of the total. It is also simpler if alignment of rig and calibration systems can

employ gravity as a reference. For some firings, such as those in vacuum chambers, this is not possible and the axis of thrust must be horizontal, entailing a greater risk of error in side thrust measurement. Such a rig was designed for use with short, light motors having thrusts of up to 50 kN and in some cases generating intentional torque.

4.2.2 Design of thrust stand

The layout is shown in Fig. 12. The motor is mounted on a large diameter, quick release flange so that it overhangs the measuring part of the rig. The motor half of the coupling flange is attached to the motor so that the rig axis defined by the normal to the flange face, passing through its centre, is coincident with the nominal thrust axis of the motor. Determination of the thrust alignment is required to be better than 0.5 mrad, necessitating alignment to better than 0.1 mrad. As the diameter of the face is 81.77 mm this implies an error of 0.008 mm between the edges of the face with respect to the normal to the motor axis. In future designs it might be better to employ three smaller widely spaced coupling flanges to reduce the accuracy needed at each face. Lateral location is by a well fitting ring around the coupling face.

To keep the rig as short and stiff as possible the main thrust flexure is attached to the other end of the coupling flange unit and thence to a combined damper and load cell unit as described previously. A cylindrical member, attached to the front of the main flexure and surrounding it, is supported by side flexures from the side load cell and damper units. If these flexures led direct to the side of the cylinder nearest to them they would exert a small couple when the system deflected under load. For this reason all the side flexures pass through the main flexure via clearance holes, and the inner thin flexure is situated on the axis of the rig. All these flexures are circular in section with a thinner section at each end for reasons previously described for plate flexures. The main load cell and damper unit is fitted with adjusters to move it in the plane at right angles to the rig axis. This adjustment is vital to the performance of the rig as any inclination of the main strut to the nominal axis of the motor results in side forces. With an effective main strut length of 550 mm, 0.1 mrad error is represented by a displacement at one end of 0.05 mm.

4.2.3 Computer corrections

To adjust to this accuracy it is necessary to apply a force along the rig axis to the same degree of accuracy and to move the base of the main measuring cell until the side forces are within acceptable limits. Owing to small, second

order non-linearities it is usually impossible to reduce the resultant side forces to less than 0.1% of the axial force, so these are then measured at a series of axial loads and recorded. They are then entered as corrections in the analysis program and each side force reading is corrected by an amount determined by the axial force at the time, interpolation being used between measured points. The change of weight of the motor is also indicated in the vertical struts and correction for this must be made by noting the zero level in each channel before and after firing and distributing the change throughout the firing in proportion to the pressure or thrust integral to that point. For a typical motor the changes of force resulting from the consumption of 2000 grams of propellant are about 40 N in the forward vertical strut and about 20 N in the rear vertical strut. If these were uncorrected they would result in an angular error of 2 mrad in a motor of 20 kN thrust and proportionately more in a motor with a smaller thrust.

A further complication is the pressure rise in the vacuum chamber during the firing, which results in changes in the load measured by all the cells. This is due to pressure acting over the effective thrust rod diameter of each load cell and any differential pressure on the damper diaphragms. It is aggravated by the need to bleed air into the load cell housings to prevent combustion gases from fouling the cells during firing. The air bleed is arranged so that the pressure is maintained at a little above that expected at the end of firing and depends to some extent on leaks from the housings, which are not completely sealed. Any such load changes are automatically compensated during analysis by the same programme which corrects for weight, as the two effects cannot be distinguished. It is reasonable to use the same correction for both as the pressure depends upon the amount of propellant consumed if temperature changes are ignored. The maximum change in pressure with the largest motor permitted in the chamber is 90 torr and the maximum apparent load change due to static tests at this pressure is 2 N. Correction is thus hardly necessary but is included automatically.

Some load cell strain gauge bridges are sensitive to air pressure, presumably because of minute air bubbles under the gauges. Tests before assembly permit the selection of transducers which have minimal sensitivity to this effect.

4.2.4 Calibration

It is not possible to use the gravity method as in the vertical rig to apply the calibration force along the rig axis and the optical method, shown in Fig. 13, is substituted. The rocket motor is replaced by an alignment unit coupled to the

same flange on the rig. Along the axis of the unit are two optical targets separated by about 300 mm and aligned to an accuracy better than 0.03 mm. These are viewed, via a 45° mirror, by a telescope mounted at right angles to the unit axis on the side of the unit. This is adjusted so that the targets appear in line, by controls which allow lateral and angular movement of the telescope. A further coupling flange, mounted on the other end of the unit, is aligned with the same degree of accuracy and has a viewing hole through its centre.

A similar alignment unit is mounted on five flexures so that it is constrained to move in a straight line along the extension of the rig axis, with its coupling flange facing the other unit and separated from it by about 1200 mm. In this unit the telescope is replaced by a light source. The supporting flexures are adjusted until the two targets are aligned with those in the other unit. The two opposed coupling faces on the units are now connected by a thrust strut with flexures at each end. A standard load cell is mounted on the other end of the second alignment unit and forces are applied to this by a Macklow-Smith capsule. It is assumed that the forces thus generated are applied along the centre lines of the two flexures in the thrust rod and because of its length, relative alignment of the ends is not required to be better than 0.12 mm. The rod is supported above its centre of gravity by a low rate spring which approximately balances its weight.

The flexures are drilled through their centres and the rod is hollow so that alignment can be checked under load, but the holes have, of necessity, to be so small that they violate the Rayleigh criterion for resolution, and therefore the two distant targets are not clearly visible. It is, however, possible to detect whether movement takes place under load.

The reaction force of the Macklow-Smith capsule is taken on a thick plate which is coupled to the main thrust block by four long, braced rods. This structure also carries the flexures supporting the second alignment unit and care must be taken in aligning the end plate if distortion under load is to be avoided. This plate is supported on balls so that it can move without restriction as the rods extend under load.

4.2.5 Static test of rig

As shown in Fig. 13 a cruciform test piece which could be attached to the rig in place of a motor was constructed. This was fitted with 7 knife edges, accurately positioned so that loads could be applied at known distances along the rig axis, or off centre to produce a torque. Weights were suspended on a pan

from the knife edges numbered in the diagrams in turn and cell outputs recorded. Table 2 shows the readings obtained, and those predicted by calculation. Agreement is generally good, remembering that 5% accuracy of side force measurement is adequate for alignment calculations. To support rig and motor weights and to withstand vibratory loads during firing, the side load cells are of 2500 N range. The worst percentage error is in strut 3 with the load on knife edge 4. This, however, is only a test of the torque reading since it is impossible with this method of loading to apply torque without a large side load, a condition which would never obtain during a firing. A better check of the effect of side loads is given by loading in positions 6 and 7.

4.2.6 Accuracy

Static loading of the rig indicates a probable accuracy of 0.2 mrad, but it is difficult to assess whether this can be achieved under dynamic firing conditions. Since the change of motor weight must be allowed for, the accuracy must depend to some extent on the ratio of thrust to motor weight as the correction is probably not exact. Recent tests with motors having a thrust (N) to charge weight (kg) ratio of about 800:1 indicate that an overall accuracy of 0.25 mrad is probable. This, of course, can only be a general statement, as the complete determination of the position of the thrust vector involves more than measurement of an angle and the overall accuracy varies with the position of the vector.

4.3 System with dual thrust axes

4.3.1 Discussion of problems with dual thrust axes

With the previous two systems it was possible to measure small deviations from axial thrust because one cell absorbed thrust in the direction of the geometric axis. The others measured only error forces (apart from interaction effects) and hence the accuracy required from them was not high. For example, to measure a 5 mrad deviation with an accuracy of ± 0.25 mrad required only 5% accuracy of reading. The analysis of errors is more complicated than this since the thrust line may be both angled and offset, so that a number of load cells contribute to the calculation of the thrust deviation and hence to the error in measurement. An analysis of probable errors for a particular case of small deviations from a single axial thrust is given in Ref. 1.

In some cases, however, the thrust direction may not be fixed, such as when two nozzles inclined towards one another are operated at different times in the firing programme. The calculation of thrust magnitude and direction then

involves contributions from all load cells, even when the thrust is perfectly aligned, so that measurement accuracy is much more critical and errors must be carefully evaluated.

4.3.2 Design of stand

To deal with this condition the load struts in the rig can be rearranged as shown in Fig. 14. This arrangement would be suitable for a liquid propellant engine thrusting upwards to avoid the risk of propellants collecting in the chambers. A typical firing rig of this type is shown in Fig. 15. This arrangement gives easy access to the rocket motor but is generally less stiff than the more conventional arrangement of struts. If the motor is suitably positioned, however, the two thrust lines can be arranged to pass through the intersections of the axes of struts b , d , e and c , d , f . In the first case struts a , c and f are not subjected to forces if the thrust is perfectly aligned, and measure only forces due to misalignment. In the second case the same is true of struts a , b and e , so that a and f may be sensitive enough to measure small forces accurately. Struts b , c and e , however, measure a small out of alignment force in one case and a component of main thrust in the other, so that if these channels are adjusted to deal with the highest load likely to be experienced by them, they may be too insensitive to measure misalignment forces when the other thrust axis is operating. This problem has been overcome in one instance by the use of dual output cells and channels with suitably adjusted gains in these positions. The appropriate channel is used in the analysis.

4.3.3 Calibration

To achieve final alignment and to obtain interaction figures, means of applying forces along the two axes with a directional accuracy of about 1 part in 10000 must be incorporated by using a tie rod with flexures at each end, one coupled to the motor mounting frame at the appropriate point and the other to a tubular strut. This strut is constrained by plate flexures to move with its axis on the thrust axis and force is applied to its other end by a screw via a standard load cell. The tie rod may be removed and the tubular strut aligned optically, using targets in the strut and motor mounting frame.

4.3.4 Impulsive loading

A further problem with this rig was an impulsive force occurring a few seconds before firing, originating in the pre-firing control system, which was of greater magnitude than the motor thrust and sufficient to damage the rig.

Because the movement due to compression of the measuring system under load was at most 0.2 mm it was not possible to clamp the rig with rigid clamps, as these might have produced damaging forces due to differential expansion of the rig even if they could have been adjusted with sufficient accuracy. The solution was to use hydraulic pistons operating in pairs, as shown in Fig. 16, each piston opposing the other and clamping the rig in all directions when hydraulic pressure was applied to them. Each opposed pair was coupled by a pipe with a restriction so that they could move with any movements of the rig and would automatically adjust their position so that forces on each side of the rig were balanced. The restriction was such that for the duration of the impulsive force the rig could move only a small proportion of the movement due to a full scale load. After the impulse and before firing the clamps were withdrawn hydraulically. The method of calculating restrictor sizes, etc., is given in Appendix 5.

4.3.5 Assessment of accuracy

It is usually necessary to know the distance by which the thrust line will miss some point in space, usually the centre of gravity of the missile system to which the rocket motor is attached. This can be calculated by measuring the angle and position of the thrust vector where it passes through the plane of struts d , e and f . This can then be resolved into an angular error and a displacement error at this plane, such that at any point along the thrust axis the miss distance varies with the angular error but includes the constant displacement error. The errors inherent in the system must therefore be assessed, particularly if the thrust lines cannot be made to pass through the strut intersections as described previously.

Consider a thrust vector passing through the measurement plane of struts d , e and f and resolve this into components in the XY and XZ planes as in Fig. 14. Using the notation of that figure

$$\tan \alpha = \frac{e + f}{a + b + c}$$

where the letters denote the forces in the struts. If the angular error is $\delta \tan \alpha$

$$\frac{\delta \tan \alpha}{\tan \alpha} = \frac{\delta e + \delta f}{e + f} + \frac{\delta a + \delta b + \delta c}{a + b + c} \quad .$$

This can be evaluated if the approximate values of all the forces and the probable measurement errors are known. The miss distance in the Y direction of the centre of gravity can then be calculated from:

$$\text{miss distance due to angular error } (\delta y') = \frac{\delta \tan \alpha}{\tan \alpha} \cdot \tan \alpha \cdot \text{distance to c of g}.$$

To calculate the displacement error:

$$\text{taking moments about the Z axis, } y = \frac{a D}{a + b + c}.$$

$$\text{Let } b + c = t$$

$$y = \frac{a D}{a + t} = D (1 + t/a)^{-1}$$

$$\therefore \delta y = \frac{\partial y}{\partial t} \delta t + \frac{\partial y}{\partial a} \delta a.$$

$$\text{Let } 1 + t/a = u \text{ then}$$

$$\frac{\partial y}{\partial t} = \frac{\partial y}{\partial u} \cdot \frac{\partial u}{\partial t} = - \frac{D}{a} (1 + t/a)^{-2}$$

$$\text{and } \frac{\partial y}{\partial a} = \frac{\partial y}{\partial u} \cdot \frac{\partial u}{\partial a} = D (1 + t/a)^{-1} t a^{-2}$$

$$\begin{aligned} \therefore \frac{\delta y}{y} &= - \frac{D (1 + t/a)^{-2}}{D (1 + t/a)^{-1}} \delta t + \frac{D t a^{-2} (1 + t/a)^{-2} \delta a}{D (1 + t/a)^{-1}} \\ &= - \frac{\delta t}{a (1 + t/a)} + \frac{t \delta a}{a^2 (1 + t/a)}. \end{aligned}$$

But since δt and δu may be positive or negative the worst case is given by

$$\frac{\delta y}{y} = \frac{\delta t + t \left(\frac{\delta a}{a} \right)}{a (1 + t/a)} = \frac{\delta (b + c) + (b + c) \frac{\delta a}{a}}{a + b + c}.$$

δy can thus be calculated and added to the miss distance due to the angular error to give the worst possible error in the Y direction. A similar analysis

in the Z direction gives a figure which when added vectorially to $\delta y + \delta y'$ gives the total miss distance x , as follows,

$$x = \sqrt{(\delta y + \delta y')^2 + (\delta z + \delta z')^2}.$$

The signal conditioning equipment used with the load cells must have sufficient resolution to achieve whatever accuracy has been assumed in the calculations although some relaxation may be possible as follows. Since each miss distance error is composed of errors from a number of cells measuring different loads, some may contribute much less than others to the overall error. This relaxation can be particularly helpful if the cell has to measure widely differing loads when the thrust axis is switched.

5 MEASUREMENT OF TRANSIENT FORCES

5.1 Theoretical discussion

A thrust measurement system in its simplest form can be represented as in Fig. 24. The mass, M , consists of the motor and any part of the rig attached rigidly to it. The load measuring transducer can be regarded as a spring reacting against a rigid structure consisting of the thrust block. In practice there is compression of the flexures coupling the transducer, some compression of the thrust block, and possibly parasitic oscillation in parts of the structure. The equation of motion of such a system may be written

$$T = M \frac{d^2 x}{dt^2} + C \frac{dx}{dt} + kx \quad (1)$$

where x is the displacement of the mass M

C is the damping coefficient

k is the stiffness of the system

T is the external applied force.

To consider the response of the system T may be replaced by an oscillatory force $F \sin \omega t$ ($\omega = 2\pi$ frequency) and the natural frequency is given by

$$\omega_n = \sqrt{\frac{k}{M} - \left(\frac{C}{2M}\right)^2}.$$

The second term, $\left(\frac{C}{2M}\right)^2$ is usually too small to have a significant effect on ω_n and can often be ignored. A set of graphs giving the natural frequency of a rig for a range of masses and stiffnesses is given in Fig. 28. Provided that ω is much less than ω_n , the first two terms in equation (1) can be ignored and kx gives a good representation of the applied force. Most firing rigs rely upon this and filter out electrically any components above about $\frac{\omega_n}{2}$. ω_n is raised to the highest practical value by keeping M to a minimum and k to a maximum. It is often impossible to raise ω_n sufficiently and it is then necessary to measure the other terms of the equation. The errors in amplitude and phase incurred by measuring only kx at various ratios of $\frac{\omega}{\omega_n}$ and at various damping ratios are shown in Fig. 17. The damping ratio, λ , is given by $\lambda = \frac{C}{C_c}$ where C_c is the critical damping coefficient at which oscillation just fails to occur when the system is shock excited. It can be seen that a reduced error in one results in an increased error in the other.

A term commonly used in the analysis of damped vibrating systems is the magnification factor, Q , given by the ratio of displacement, x_n , of the mass for a given driving force at resonance, ω_n , to the steady displacement, x_o under the same constantly applied force, i.e.

$$Q = \frac{x_n}{x_o}.$$

Another way of expressing the same thing is the bandwidth, B , which is the width of the resonance peak in angular measure between levels at 0.707 of the peak amplitude. Q is also given by

$$Q = \frac{\omega_n M}{C} = \frac{\omega_n}{B}$$

and all these terms may be used in the design of thrust rigs. Fig. 18 gives a useful set of graphs relating Q , bandwidth, number of cycles to $\frac{1}{2}$ amplitude and mass per damping force at unit velocity for a range of rig natural frequencies.

5.2 Complete evaluation of equation of motion

5.2.1 Practical rig construction and signal conditioning

Rigs have been constructed in which a load cell forms the spring, an accelerometer measures the $M \frac{d^2x}{dt^2}$ term, and the force generated by two damper pistons (described in Section 3.2) is measured by load cells. The outputs of all these devices are summed by amplifiers and networks to give a true representation of T throughout the firing. The value of the term $C \frac{dx}{dt}$ measured by such a system may be in error if other damping is present and it may then be better to derive the term from another measured term.

If the system is oscillating

$$x = A \sin \omega t \quad \text{where } A \text{ is the amplitude of oscillation}$$

$$\frac{dx}{dt} = A\omega \cos \omega t$$

$$\frac{d^2x}{dt^2} = -A\omega^2 \sin \omega t \quad .$$

$\frac{dx}{dt}$ can be obtained by differentiating x or by integrating $\frac{d^2x}{dt^2}$. In practice the latter course has been found preferable because any noise spike on the x signal results in a large value of $\frac{dx}{dt}$, whereas noise in $\frac{d^2x}{dt^2}$ is diminished by integration.

A block diagram of the signal conditioning equipment is shown in Fig. 19. The output from the load cell is buffered by an operational amplifier (No. 1) in which the gain may be varied between 0.1 and 10000. These amplifiers are used throughout and were chosen to have a high input impedance (100 M Ω), 140 db common mode rejection ratio and low offset drift of 1 $\mu\text{V}/^\circ\text{C}$. The output from the accelerometer goes to a similar amplifier (No. 3) and both amplifiers feed into opposite differential inputs of a further amplifier (No. 4) which adds them vectorially.

If the damping force is measured directly, the load cell which measures it feeds to a third amplifier (No. 2) and the outputs from this and from amplifier No. 4 are again mixed in amplifier No. 5. Resonance of the individual transducers may cause the combined output to contain unwanted high frequencies which limit the upper frequency response of the system. The final mixed signal is therefore

fed via a buffer to a low pass filter stage which can be set to cut at any desired point in the frequency range of the equipment.

If damping force is not measured it is derived by feeding some of the $M \frac{d^2x}{dt^2}$ output from amplifier No. 3 to amplifier No. 6 which has a suitable integrating network operating over the frequency range 50 Hz to 1500 Hz. The low frequency response is limited to prevent the integrator from running out of range and in any case damping forces are expected to be low in this region. The output of amplifier No. 6 can be switched into the input of amplifier No. 4 in place of that from the damper amplifier, No. 2.

5.2.2 Calibration

The gains of the appropriate amplifiers must be adjusted to represent the values of k , C and M and it is possible, if tedious, to determine these individually and set up each amplifier. In practice this would be difficult and an empirical system based on the response of the rig to shock excitation is used. The shock is produced by striking the rig in an axial direction, preferably with an instrumented hammer containing a piezoelectric element which records the force and has a high natural frequency.

The kx channel is first calibrated and adjusted using static loads produced by deadweights or by methods described elsewhere in this report. The rig is then shock excited with the gain in the $C \frac{dx}{dt}$ channel set at zero. The gain of the $M \frac{d^2x}{dt^2}$ channel is adjusted to produce a minimum in the $M \frac{d^2x}{dt^2} + kx$ combined output. The $M \frac{d^2x}{dt^2}$ and kx signals are 180° out of phase with each other and the minimum combined signal is at 90° to each, as is the $C \frac{dx}{dt}$ signal. The $C \frac{dx}{dt}$ signal is now adjusted so that it just cancels out the remaining signal. The impulse recorded should now be a replica of that indicated by the instrumented hammer. Any higher frequency components present may now be filtered out by adjusting the cut-off point of the final filter circuit.

5.2.3 Practical problems and results

The practical problems in the use of such an arrangement are that rigs may have more than one resonant frequency, particularly when feed pipes and other connecting devices are required, and that few behave as a simple spring and mass system. Every attempt should be made to keep the rig simple to obviate these troubles, but if this is not possible the transfer function of the conditioner

can be suitably adapted. In the simplest case, notch filters may be used to remove unwanted resonances and if they are sufficiently narrow they need not cause unacceptable distortion in the final output.

Fig. 20 shows the uncompensated response of a typical rig to an impulse, i.e. the signal produced by the load cell in the kx channel. Fig. 21 shows the response to the same impulse when both $M \frac{d^2x}{dt^2}$ and $C \frac{dx}{dt}$ channels are correctly adjusted.

5.3 Ballistic measurement of impulse and thrust

5.3.1 Basis of the ballistic approach

An alternative to measuring or deriving all the terms of the equation of motion of a firing rig, when it is not possible to raise the natural frequency sufficiently, is to reduce the stiffness and damping to zero. The equation of motion of the previous section then reduces to $T = M \frac{d^2x}{dt^2}$ and it is necessary to measure only the acceleration of the motor and any mass attached to it. This is a practical solution only when the total impulse of the motor is small if the necessary mass to which the motor is attached is to be kept within practical limits. This constraint limits the usefulness of the technique to motors having burning times of tens of milliseconds at current thrust levels.

5.3.2 Ballistic measuring systems

Various ballistic measuring systems have been used to measure short duration forces, the most common being the ballistic pendulum. This was initially considered to be a solution to the problems of thrust measurement in motors with high thrust and short burning times. It depends upon the fact that in the absence of other forces:

$$\int_0^t F dt = MV$$

where F is the instantaneous thrust

t is the time for which the thrust acts

M is the moving mass

V is the final velocity assuming the mass to be initially at rest.

This is true if the mass and pendulum length are sufficient for the mass to move negligibly during the impulse. The impulse is deduced by measuring the

final position of the mass at the peak of its swing. Usually its increase in height is measured directly or indirectly to give its gain in potential energy, which is equal to the initial kinetic energy and hence the impulse is known. A thrust/time curve may be obtained from an accelerometer mounted on the pendulum, but the accuracy is limited and calibration is difficult. An analysis of this simple case is given in the first part of Appendix 6.

Appendix 6 then considers the case in which displacement of the mass during the impulse is significant, so that allowance must be made. Its displacement must be measured at the end of thrust as well as at maximum swing. This assumes that the thrust can be considered to rise and fall instantaneously and remain at a constant value when applied. A real rocket motor is likely to generate a thrust which varies with time, so that F must be known as a function of displacement and measured with an accelerometer. Acceleration and velocity may also be derived by direct measurement or by appropriate differentiation of displacement along the arc of swing, but accuracy is not likely to be great.

The practical problems involved in the realisation of an accurate device are considerable. The mass of the pendulum, including anything attached to it must be known, and this changes with consumption of the motor charge. With a reasonable pendulum length the mass must be large (about 1000 kg with current motors) to minimise travel during the burning time. This involves a suspension having a substantial mass and this, with the finite size of the main mass, means that the moment of inertia of the combination about the pivot must be calculated or measured. A parallel motion suspension avoids the problem of the distributed mass of the pendulum, but the inertia of the suspension must be known.

Determination of the position of the centre of gravity of the mass at its maximum swing is difficult and allowance may be necessary for any motion in directions other than the intended direction of swing. This is particularly important if the measuring point on the mass is not at the centre of gravity and there is rotation about the centre of gravity. It is convenient to measure angular swing near the pivot, but there must be no bending or vibration in this region if errors are to be avoided. Frictional losses in the bearings needed to support the large mass may have to be evaluated, probably by measuring successive swings, and some means of arresting the pendulum must be provided.

Most of these problems can be overcome by allowing the mass to move horizontally after the impulse, and measuring the integral of the force required to bring it to rest.

5.3.3 Description of system

The system finally selected is shown in Fig. 22. It consists of a mass M , the value of which need be known only approximately, supported on three low friction linear bearings sliding on horizontal rods. The motor to be tested is mounted on the rear face of the block so that it accelerates the mass along the rods for a short distance without resistance during the motor firing. An accelerometer mounted in the block on the motor axis near the front face produces a thrust/time curve since $F = Ma$, where a is the acceleration. It is situated in this position to keep it as remote as possible from shock excitation from the rocket motor. The mass of the block is approximately 1000 kg to ensure reasonable lengths of travel during the firing time and reasonable final velocities with motors in the impulse range of 400 to 1500 Ns for which the equipment was designed. Since the block is approximately a 500 mm cube its lowest resonant frequency is such that $\lambda = 1 \text{ m}$, i.e. 5 kHz. If this frequency is excited a low pass filter must be incorporated in the recording system to cut at a suitable frequency below this value. The accelerometer used in the initial experiments is an Endevco Model 2262-1000 piezo resistive type to match into existing instrumentation. It has an output of 0.5 mV per g and a natural frequency of 6 kHz, response being flat to within $\pm 5\%$ from 0 to 2000 Hz. This latter characteristic governs the cut-off frequency of the thrust measuring system in most cases.

After the end of motor burning the mass travels a short distance and is then brought to rest by a device which applies a constant decelerating force for a time which is inversely proportional to the magnitude of the force and is chosen to be such that normal recording and integrating systems can be used. A typical combination is 4000 N for 250 ms resulting from a motor impulse of 1000 Ns.

The initial decelerating device was designed as an oil filled piston and cylinder pressurised to a pre-selected value from a nitrogen gas reservoir large enough to prevent the pressure from altering significantly during the arresting period. This design is described in Appendix 7 as it may be required if difficulty is experienced with the device now employed.

Subsequently, a commercial device was found to exist, in which the cylinder is perforated with a series of adjustable orifices which are closed in turn by the piston to achieve a similar effect. This is shown in Fig. 23. The device is mounted on the end of the frame carrying the rods which support the mass.

The frame is supported by flexures and coupled by a rod flexure to a load cell and damper unit which measures the force applied to the decelerator. The time integral of this force is equal to the motor total impulse if there are no losses in the system.

5.3.4 System accuracy

Friction of the linear bearings could cause inaccuracy although their coefficient of friction is probably less than 0.005 when they are in good condition. To avoid such errors, whatever the condition of the bearings, the support rods are mounted on flexures so that the load cell measures the frictional forces generated in the bearings. Frictional forces in the retarding device are also measured by the cell so that losses from these effects are negligible.

The accuracy of measurement of total impulse depends on the load cell and recording devices. Since the retarding device gives rise to a sensibly constant decelerating force, the load cell may be operated close to its working maximum and should hence be capable of an accuracy of 0.1%. Digital recording and analysis devices used are capable of an accuracy of better than 0.1%. The cell is calibrated with a standard cell of 0.05% accuracy to achieve an overall accuracy of 0.2% in total impulse measurement.

Any stored elastic energy in the measuring system or retarding device may result in the mass acquiring a small velocity in the reverse direction after its arrest. If this is significant it is necessary to latch the mass to the arrester when it makes contact and to subtract from the integral any negative thrust produced during the final rebound.

The error in accelerometer measurement of thrust may be evaluated as follows. Let the permissible error be 1% and assume a coefficient of friction of 0.01. Since the mass is 1000 kg the frictional force is approximately 100 N, so that the minimum thrust is 10000 N to achieve 1% accuracy. If the total impulse is known to within 0.2% a greater error than 1% in thrust is probably acceptable as the shape of the thrust curve is usually more important than spot readings. Accuracy is probably limited by the accelerometer to $\pm 5\%$ for the higher Fourier components of the thrust transient, but can be shown to be within this limit provided that the rise time of the rocket motor thrust is not less than 2 ms. Except during the thrust transient an accuracy of $\pm 2\%$ is achieved.

Air drag is negligible since the force on the block at maximum velocity with the greatest total impulse envisaged is about 3 N, and since this acts for 20 ms at most the error in impulse is 0.06 Ns.

5.3.5 Use of the equipment

If it is assumed that a motor of total impulse I Ns and maximum thrust F Newtons is to be tested the thrust at the load cell must be spread over about 0.25 sec or longer to permit a sufficiently accurate integration of the thrust. The range of the load cell must thus be such that it can measure accurately a force, F_1 , where

$$F_1 = \frac{I}{0.25} \text{ N} .$$

The linear decelerator must be adjusted to provide this decelerating force.

The maximum acceleration of the mass is given by

$$a = \frac{F}{10^3} \text{ m sec}^{-2}$$

so that the gain of the accelerometer amplifier must be set to accommodate the accelerometer output at this value.

The load cell must be calibrated in the usual manner with reference to the site standard.

The mass must be in its starting position and the motor attached to it firmly. To obtain an accurate thrust representation all mating surfaces must be machined flat to the best engineering tolerances and a film of grease may be applied to take up any remaining clearance between surfaces.

Recording of load cell output must be by a digital system with a resolution of better than 1 part in 1000, and a sampling rate of not less than 1 kHz and preferably above 5 kHz.

The accelerometer measurement must be recorded by a digital system with a sampling rate of at least 10 kHz or by an analogue system with a flat response to 2 kHz.

The thrust integral is obtained directly from the digital recording of the load cell output. The accelerometer recording can be integrated in terms of trace displacement, d , against time, t . Thus, for the accelerometer calibration constant, K :

$$K \int d \, dt = \int F dt = I$$

$$\therefore K = \frac{I}{\int d \, dt}$$

No direct calibration of the accelerometer is therefore required.

5.3.6 Summary of advantages

This equipment permits measurement of the total impulse of motors with short burning times, with the same accuracy and using the same auxiliary equipment as for motors with long burning times. The thrust/time curve can be recorded using an accelerometer which need not be directly calibrated. It is easier to use and avoids most of the errors inherent in a ballistic pendulum. The mass must be known with only sufficient accuracy to permit adjustment of the range of the measuring systems, and only a static calibration of the load cell is required. It is capable of measuring total impulse with an accuracy of $\pm 0.2\%$ and instantaneous thrust, within frequency limitations, to $\pm 2\%$.

5.4 Transient behaviour of system measuring only displacement

5.4.1 Discussion of rig response

Most thrust measuring systems record only the displacement term of the equation of motion so that it is important to know their limitations when transient phenomena are recorded. The most critical part of a rocket motor thrust curve is the initial rise as this usually contains the highest frequency components. The following analysis therefore deals with system response to this part of the curve, but the results can be applied to other rapid changes if suitable modifications are made.

Any degree of accuracy can be achieved if the natural frequency of the measuring system sufficiently exceeds the highest frequency component of the transient. Often this is not possible, particularly when thrust is measured because the moving mass and the stiffness of the measuring system combine to limit the attainable natural frequency. In these cases a compromise must be accepted in the form of a natural frequency lower than that desired and application of suitable damping. Some distortion in the resulting record is inevitable and it is important to know the probable error as some correction may be possible.

The dynamic response of systems has been treated theoretically in many textbooks, but it is not always easy to apply the solutions to practical problems.

In particular, the operator on a firing site does not have time to apply theoretical solutions to each of his measuring problems and this section aims to mitigate this difficulty. The initial part involves a mathematical solution from which design criteria may be drawn, but it is not necessary to follow this to select a suitable measuring system.

This is followed by the results of experiments with an electrical analogue, which show pictorially the response achieved with systems having different natural frequencies and different degrees of damping. Finally, graphs are drawn from which it is possible to determine the system required to achieve a given accuracy of amplitude measurement at different parts of the initial transient, and an acceptable delay in response.

5.4.2 Mathematical solution

To apply a mathematical solution the conditions must be idealised, and the model used is as follows.

- 1) The measuring system approximates to a mass attached to a spring with damping proportional to the velocity of the mass (Fig. 24). (If this model is chosen so that its natural frequency corresponds to the lowest resonant frequency of the measuring system this is a reasonable assumption.) The equation of motion of such a system is

$$M \frac{d^2x}{dt^2} + \frac{Cdx}{dt} + kx = 0$$

or

$$\frac{d^2x}{dt^2} + 2n \frac{dx}{dt} + \omega^2 x = 0$$

where

$$n = \frac{C}{2M} \quad \text{and} \quad \frac{k}{M} = \omega^2$$

the rest of the symbols being defined below.

- 2) The driving force consists of a ramp function rising linearly with time. (This is probably more severe than the real case, in which pressure and thrust are likely to rise less rapidly initially.)

Fig. 25 shows the model and the drive function rising from zero to a steady value between time $t = 0$ and $t = t_{\max}$ and having the value of Kt where K is a constant. The response of such a model to this function is given by

$$F = Kt + \frac{2 Kn (e^{-nt} \cos \omega_1 t - 1)}{n^2 + \omega_1^2} + \frac{K (n^2 - \omega_1^2) e^{-nt} \sin \omega_1 t}{\omega_1 (n^2 + \omega_1^2)^2}$$

where $F = kx$

$k =$ spring stiffness

$x =$ displacement of the mass

$M =$ mass

$\omega =$ undamped natural frequency in radians/sec $= 2\pi f_n$

$f_n =$ undamped natural frequency in Hz

$\omega_1 =$ damped natural frequency $= \omega \sqrt{1 - h^2}$

$h = \frac{C}{C_{crit}} = \frac{\text{damping constant}}{\text{critical damping constant}}$

$n = \omega h$

The spring corresponds to the measuring element in the system and the output is proportional to F with most simple systems.

The ratio of measured force to applied force is a measure of the error of the system, E , so that we may write

$$E = \frac{F}{Kt} = 1 + \frac{2n (e^{-nt} \cos \omega_1 t - 1)}{t (n^2 + \omega_1^2)} + \frac{(n^2 - \omega_1^2) e^{-nt} \sin \omega_1 t}{t \omega_1 (n^2 + \omega_1^2)^2}$$

Substituting ωh for n and $\omega \sqrt{1 - h^2}$ for ω_1

$$E = 1 + \frac{2\omega h (e^{-\omega h t} \cos t \omega \sqrt{1 - h^2} - 1)}{t [\omega^2 h^2 + \omega^2 (1 - h^2)]} + \frac{[\omega^2 h^2 - \omega^2 (1 - h^2)] e^{-\omega h t} \sin t \omega \sqrt{1 - h^2}}{t \omega \sqrt{1 - h^2} [\omega^2 h^2 + \omega^2 (1 - h^2)]^2}$$

Simplifying and writing $\omega = 1$ gives

$$E = 1 + \frac{2h (e^{-ht} \cos t \sqrt{1 - h^2} - 1)}{t} + \frac{(2h^2 - 1) e^{-ht} \sin t \sqrt{1 - h^2}}{t \sqrt{1 - h^2}}$$

This may be evaluated to give the curve of E throughout the rise time of the drive function Kt . What is more often required is the deviation, δ , of the curve of F from the ramp Kt at all points during the rise time and in particular and maximum deviation. This may be expressed as a fraction of the maximum value of the ramp function Kt_{\max} at time t_{\max} as this is usually more meaningful than $\frac{\delta}{Kt}$, particularly at small values of Kt . Fig. 25 shows that

$$\frac{\delta}{Kt} = 1 - \frac{F_t}{Kt} \quad \text{when } F_t \text{ is the value of } F \text{ at time } t$$

so that

$$\frac{\delta}{Kt_{\max}} = \frac{\left(1 - \frac{F_t}{Kt}\right) t}{t_{\max}} = \frac{(1 - E_t) t}{t_{\max}}.$$

If we wish to specify a maximum permissible fractional error, Δ , for $\frac{\delta}{Kt_{\max}}$ we may write this expression as

$$\Delta = \frac{(1 - E_t) t}{t_{\max}}$$

when

$$t_{\max} = \frac{(1 - E_t) t}{\Delta}.$$

It is now necessary to relate the duration of the rise, t_{\max} , to the natural frequency of the measuring system required to keep the fractional error below Δ . We have

$$f_n = \frac{1}{\tau} = \frac{\omega}{2\pi}.$$

Where τ is the period of one cycle at the natural frequency, and since ω has been taken to be 1

$$f_n = \frac{1}{\tau} = \frac{1}{2\pi}$$

therefore we may write

$$\frac{t_{\max}}{\tau} = f_n t_{\max} = \frac{(1 - E_t) t}{2\pi \Delta} .$$

The use of the function $\frac{t_{\max}}{\tau}$ or $f_n t_{\max}$ is convenient as it is independent of the actual values of t_{\max} or τ and depends only on the ratio of the two. It is justified because the shape of the response is governed only by this ratio, so that graphs of error against this function apply whatever the actual value of t_{\max} .

Inserting the expression for E the above equation becomes

$$f_n t_{\max} = \frac{2h (e^{-ht} \cos t \sqrt{1 - h^2} - 1)}{2\pi \Delta} + \frac{(2h^2 - 1) e^{-ht} \sin t \sqrt{1 - h^2}}{2\pi \Delta \sqrt{1 - h^2}} .$$

This was evaluated for $h = 0.1$ to 0.9 representing lightly damped to over damped systems, each for a suitable range of values of t . The worst amplitude error, expressed as a percentage of the maximum amplitude ($K t_{\max}$) occurs near the start of the rise and graphs are plotted in Fig. 26 of the percentage error at this worst point against the product of the natural frequency of the measuring system and the rise time ($f_n t_{\max}$). The graphs are drawn for different damping ratios and for errors down to 1%, but because they are straight lines on log/log scales, extrapolation to smaller errors is simple. The graphs are linear as t_{\max} decreases to the point at which t is equal to the time when the maximum error is measured. At lower values of t_{\max} the worst error is at t_{\max} and all the curves converge as t_{\max} decreases.

If this initial error is unimportant and the error further up the rise time is the critical factor, some relaxation of the requirements for the measuring system is possible. This is significant only for damping factors below about 0.5 and two graphs have been plotted for $h = 0.2$ and 0.4 to illustrate this.

If the worst delay, expressed as a percentage of the rise time (t_{\max}), is required this has the same value as the amplitude percentage error and may be read from the graphs in the same manner. It must be remembered that f_n and t_{\max} must be expressed in the same units and to avoid confusion f_n should be expressed in cycles per second and t_{\max} in seconds.

If the error during the rise time has been kept within bounds it is still necessary to ensure that the overswing, in cases where damping is less than critical, is also within acceptable limits. Graphs obtained from the analogue recordings are shown in Fig. 27 and it may be seen that if the error criterion for the rise time has been met, the overswing in all practical cases involves a smaller error. The exception is for very low damping, when the overswing depends upon the phase of the oscillatory signal when the input rise terminates. The distortion in the graph for $h = 0.07$ is due to this.

5.4.3 Determination of damping ratio

In many cases the natural frequency and damping ratio of a measuring system cannot be changed and the characteristics of the system must be determined so that probable errors may be evaluated. A simple method of accomplishing this is to shock excite the system into oscillation by any convenient method and record the decaying oscillation.

The natural frequency of the system can be measured from the record, remembering that it is the damped angular frequency ω_1 , which is recorded, although this does not differ significantly from ω except for heavy damping. Graphs of undamped natural frequency against rig stiffness are given in Fig. 28 for a range of moving masses (motor weight plus any part of the rig which deflects with the motor under load). The amplitude of each peak in the decaying oscillation bears a constant relationship to the subsequent peak, the Napierian logarithm of this ratio being termed the logarithmic decrement of the system. If x_1 is the amplitude of the first peak and x_2 that of the second it may be shown that

$$\log_n \frac{x_1}{x_2} = \frac{2\pi h}{\sqrt{1-h^2}} \quad .$$

A graph of the ratio x_1/x_2 against h is given in Fig. 29, from which the value of the damping ratio, h , may be obtained, given x_1/x_2 .

Any check of the system should include all parts of it; amplifiers, filters, recorders, etc., as these may each modify the response and a check of any one part, such as the transducer, may give a totally false impression. A common case is that of a pressure transducer having a very high natural frequency and low damping, used with a recording system with a lower cut-off frequency, so that the overall system behaves as if the system were critically damped. It must also be

remembered that a pressure transducer should be tested with any coupling pipe placed exactly as it is used.

Examples of the use of the graphs are given in Appendix 8.

5.4.4 Use of electrical analogue

The equation of motion of the damped spring and mass system forming the measuring device is

$$M \frac{d^2x}{dt^2} + C_m \frac{dx}{dt} + kx = 0$$

in the absence of a driving force.

The equation governing the flow of charge in an electrical damped tuned circuit is

$$L \frac{d^2Q}{dt^2} + R \frac{dQ}{dt} + Q \frac{1}{C} = 0$$

or more commonly

$$L \frac{di}{dt} + Ri + \int i dt \frac{1}{C} = 0 ,$$

where L is the inductance in henries

R is the resistance in ohms

C is the capacitance in farads

Q is the charge

i is the current in amps .

It may be seen that there is an exact analogue between electrical and mechanical units, so that the behaviour of a mechanical system may be simulated by an electrical circuit in which the values are more easily and rapidly changed. The theoretical treatment previously described considered only the behaviour of the system while the ramp input was rising, whereas in a real case the behaviour when the rise terminates is equally important. Moreover, any complication of the theoretical treatment becomes very involved and must entail the use of idealised pulse shapes, etc. In the electrical analogue these constraints do not apply so that very rapid solutions are possible. The accuracy of the analogue technique is less than that with a computer solution of the theoretical

equations, but it is usually more than adequate to deal with a real case in which the system response may not be ideal.

The analogue circuit consists of a lightly damped inductor of 0.1 H, a capacitor of 0.25 μ F and a variable resistor of 1000 Ω as shown in Fig. 30. The input waveform is injected across a 0.5 Ω resistor in the resonant loop via a 50 Ω resistor to avoid feedback from the resonant loop into the ramp generator. The input is measured at the ramp generator and the output across the capacitor by a high impedance oscilloscope, the charge on the capacitor being equivalent to the displacement of the mass of the mechanical system. These components give a resonant frequency of 1 kHz which is similar to that of many measuring systems, although this is of very little consequence unless recording systems are to be tested when coupled to the analogue circuit. Variation of the resistor permits damping to be changed over a wider range than is likely to be encountered in practical mechanical systems.

A commercial ramp generator is used in which the slope of the ramp may be selected as required. The input ramp and the voltage across the capacitor are displayed on separate traces of an oscilloscope which are adjusted so that the baselines and the deflected traces under steady conditions are coincident. The deviation of one trace from the other is thus a measure of the error in the measuring system.

5.4.5 Results

A series of photographs of the oscilloscope traces, taken with different degrees of damping and different slopes of the input ramp, is shown in Figs 31 to 34. The results are applicable at any resonant frequency, provided that the ratio of the period of this oscillation to the rise time is the same or, in other words, that the product of frequency and rise time is constant. The application of these results to a particular case must depend upon what information is required from the record, but three items are commonly of particular interest:

- 1) the maximum amplitude error occurring during the rise time as a proportion of the steady deflection;
- 2) the maximum amplitude error occurring after the termination of the rise time expressed in the same way;
- 3) the maximum delay in the measured rise expressed as a proportion of input rise time.

These have been measured from the traces and agree with the theoretical figures on which the graphs are based. The graphs are based only upon particular points of measurement and the pictures of the response should be consulted to ensure that these points of measurement are significant in each case. For example, whereas a 10% overswing may be acceptable, a following train of decaying oscillation may not be. If values are obtained by measurement from the traces accuracy is not high but is nevertheless usually sufficient.

The values obtained by analogue techniques agree reasonably well with those calculated theoretically, as would be expected. The damping ratio of 0.64 usually recommended is a good compromise in most cases, but delay may be reduced by using a lower damping ratio, such as 0.3. This is quite acceptable provided that the input waveform is not steep enough at any time to contain appreciable Fourier components at f_n , when overswing of up to 45% is possible.

With certain combinations of parameters it is possible to record a waveform rising at the same rate as the input waveform but displaced in time. This could be particularly misleading as the response appears to be adequate from rise time measurements and it is even possible to obtain the appearance of a rise time faster than the input.

The linear rising ramp is probably a more severe test than the waveforms generated by rocket motors because the rate of pressure rise is probably lower initially than later in the pressure build-up. The electrical tests could be repeated with different waveforms and may be used to predict the behaviour of a measuring system or to reconstruct the input waveform from a recorded waveform.

6 CONCLUSIONS

By the proper use of techniques described in this report it is possible to measure thrust levels and total impulses of rocket motors to an accuracy better than 0.2%. Thrust alignment at ambient pressure can be determined to about 0.2 mrad and under vacuum conditions with small motors to about the same accuracy, provided that the burning time is not less than about 150 ms. Techniques are available using dynamic techniques, or by suitable signal conditioning, for measuring total impulse of motors with very short burning times. In this latter field there is room for further improvement and modern micro-circuits will permit complex operations to be carried out at reasonable cost.

7 REFERENCE

<u>No.</u>	<u>Author</u>	<u>Title, etc.</u>
1	Dean, D.S. Lyons, E.A. Norman, D.R.	A six-component stand for thrust vector control experiments with rocket engines. RPE Technical Report No. 67/12 (1967)

APPENDIX 1

Stiffness of flexure units

Consider a unit as shown in Fig. 35, consisting of two flexible strips of length Δ , width b and thickness d rigidly coupled to a stiff bar and rigidly clamped at their outer ends to surfaces which are separated by distance h . With these surfaces parallel let forces W be applied to them such that the unit is deflected through a distance X .

As the system is symmetrical about the centre of the bar there can be no resultant couples acting on the bar after the deflection since any couples due to the strips would act in the same sense and rotate the bar until they were zero. If the bar were cut in the centre we would thus have forces W acting at the cut surface as in Fig. 36. For small deflections we can thus regard each half as a cantilever acted upon by a force W at a distance $h/2$ from its fixed end and stiff from a distance Δ from the fixed end to the point of application of the force.

Let the deflection at the end of the strip be y .

Let the slope at this point be θ .

Let Young's modulus of the bar be E .

Then

$$\frac{X}{2} = y + \left(\frac{h}{2} - \Delta \right) \theta \quad \text{for small values of } \theta$$

$$y = \frac{2 W \Delta^2}{E b d^3} \left(\frac{3h}{2} - \Delta \right) .$$

Using the area-moment proposition

$$\theta = \frac{6 W \Delta (h - \Delta)}{E b d^3}$$

or

$$\theta = \frac{W \Delta}{2 I E} (h - \Delta)$$

where I is the moment of inertia of the flexure section in the general case, therefore

$$\begin{aligned}
\frac{X}{2} &= \frac{2 W \Delta^2}{E b d^3} \left(\frac{3h}{2} - \Delta \right) + \left(\frac{h}{2} - \Delta \right) \left(\frac{6 W \Delta [h - \Delta]}{E b d^3} \right) \\
&= \frac{W \Delta^2}{E b d^3} (3h - 2\Delta) + \frac{6 W \Delta}{E b d^3} \left(\frac{h}{2} - \Delta \right) (h - \Delta) \\
&= \frac{W \Delta}{E b d^3} (3h \Delta - 2\Delta^2) + 6 \left(\frac{h^2}{2} - \frac{3\Delta h}{2} + \Delta^2 \right) \\
&= \frac{W \Delta}{E b d^3} (3h \Delta - 2\Delta^2 + 3h^2 - 9\Delta h + 6\Delta^2) \\
&= \frac{W \Delta}{E b d^3} (4\Delta^2 - 6\Delta h + 3h^2)
\end{aligned}$$

or

$$W = \frac{X E b d^3}{2\Delta (4\Delta^2 - 6\Delta h + 3h^2)} .$$

In the general case

$$W = \frac{6 X E I}{\Delta (4\Delta^2 - 6\Delta h + 3h^2)} .$$

To compare the stiffness of rectangular and circular section flexures, let the circular section have a diameter D . For equal section areas

$$bd = \frac{\pi D^2}{4}$$

or

$$D^4 = \frac{16 b^2 d^2}{\pi^2} .$$

$$I \text{ for a rectangular section} = \frac{bd^3}{12}$$

$$\begin{aligned}
 I \text{ for a circular section} &= \frac{\pi D^4}{64} = \frac{\pi \cdot 16 b^2 d^2}{\pi^2 \cdot 64} \\
 &= \frac{b^2 d^2}{4 \pi} \text{ if the circular section has the same} \\
 &\quad \text{area as the rectangular section.}
 \end{aligned}$$

Let $b = xd$, then for equal I in the circular and rectangular sections

$$\frac{bd^3}{12} = \frac{b^2 d^2}{4 \pi}$$

or
$$\frac{xd^4}{12} = \frac{x^2 d^4}{4 \pi}$$

or
$$x = \frac{\pi}{3} .$$

Thus for flexures which take an equal tensile or compressive load (assuming no buckling) a rectangular flexure is less stiff in bending provided that $x > \frac{\pi}{3}$.

APPENDIX 2

Damping force generated by axially moving piston

Consider a piston of diameter d in a cylinder with radial clearance $h \ll d$, the gap being filled to a depth y with fluid of viscosity μ . If the piston moves axially downward with velocity v such that the fluid mean velocity in the gap is V ,

$$V = \frac{h^2}{12 \mu} \frac{dp}{dy} = \frac{h^2 (p_1 - p_2)}{12 \mu y},$$

p_1 and p_2 being respectively the pressures below the piston and at the free surface. If p_0 is taken as gauge pressure and the free surface is at atmospheric pressure

$$V = \frac{h^2 p_1}{12 \mu y} \quad (1)$$

The area of the piston is $\frac{\pi d^2}{4}$ and that of the free surface is $\pi d h$; hence

$$\frac{v}{V} = \frac{4 \pi d h}{\pi d^2} = \frac{4h}{d}.$$

Thus

$$v = \frac{vd}{4h} = \frac{d}{4h} \quad (\text{when } v \text{ is unit velocity}) \quad (2)$$

Substituting (2) in (1)

$$\frac{d}{4h} = \frac{h^2 p_1}{12 \mu y}$$

or

$$h^3 = \frac{3d \mu y}{p_1} \quad (3)$$

To obtain the clearance for critical damping of a spring and mass system of mass M , angular frequency of oscillation ω and damping force C at unit velocity

of the piston we have

$$p_1 = \frac{C}{\pi d^2} \quad (4)$$

but for such a system $C = 2M \omega$ so

$$p_1 = \frac{8M \omega}{\pi d^2} \quad (5)$$

Substituting (5) in (3) gives

$$h = \sqrt[3]{\frac{3\pi \mu d^3 y}{8M \omega}} \quad .$$

The axial force on the piston at unit velocity is given by

$$T_A = p_1 \frac{\pi d^2}{4} v \quad .$$

Substituting for p_1 from (3) gives

$$T_A = \frac{3\pi d^3 \mu y v}{4h^3} \quad .$$

APPENDIX 3

Effects of strut misalignment

Main strut

The main strut is by far the most critical as it has to resist a large force. It may be misaligned in two ways or by a combination of these, i.e. it may be vertical but displaced to one side, or it may be at an angle to the vertical. In the former case, if it is displaced by a distance a from the motor axis, a truly axial motor thrust produces a couple Ta acting about the end of the main strut. This is largely resisted by the upper strut with a moment arm b such that

$$Ta = T_1 b \quad .$$

Inserting the probable figures $T = 5000 \text{ N}$, $T_1 = 0.5 \text{ N}$ (maximum permissible error in side force measurement) , $b = 1 \text{ m}$,

$$a = \frac{0.5 \times 1000}{5000} = 0.1 \text{ mm (0.004 inch)} \quad .$$

By accurate machining this should be easy to achieve.

If the strut is at an angle to the vertical ψ a side thrust of $T \sin \psi$ is generated; but

$$\sin \psi = \frac{a'}{y}$$

where a' is the displacement of the lower end of the strut from the vertical and y is the length of the strut, say 300 mm (12 inches). Inserting the above values, we obtain

$$a' = \frac{0.5y}{T} = \frac{0.5 \cdot 300}{5000} \approx 0.03 \text{ mm (0.0012 inch)} \quad .$$

Alignment to this accuracy on site is not possible with readily available equipment and in any case the effective axis of the main strut flexures may be displaced by more than this from the geometric axis.

After adjustment to within 0.1 mm (0.004 inch) by levels and straight edges the final adjustment must be made by applying a load, similar to the motor thrust, exactly along the line which will be occupied by the motor axis. Any

misalignment of the strut produces side loads which must be kept to a minimum.

Side struts

To demonstrate that the result of misalignment of the lateral struts is far less severe it is sufficient to consider one of a number of possible consequences. Let the axial thrust T be displaced a distance a from the geometric axis of the motor. In a real rig the effective centre of rotation of the inner flexure of the side struts may be displaced from the main strut axis by a distance c' .

If the struts are perfectly aligned the forces in them are as in Fig. 37a, i.e. in the main strut, the force T_m , in the side struts the forces T_1 and T_2 .

Taking moments about A gives

$$-Ta + T_1 b = 0, \quad (1)$$

about B gives

$$T(c' - a) - T_m c' + T_1 b = 0, \quad (2)$$

and about C gives

$$T(c' - a) - T_m c' - T_2 b = 0. \quad (3)$$

From these equations $T_1 = \frac{Ta}{b} = -T_2$ and $T = T_m$ which is obvious by inspection.

If we now assume the upper strut to be misaligned by an angle θ as in Fig. 37b and the forces to be T_m in the main strut, T_3 in the upper strut and T_4 in the lower strut, taking moments about A gives

$$b T_3 \cos \theta + c' T_3 \sin \theta - Ta = 0, \quad (4)$$

about B gives

$$T(c' - a) - T_m c' + b T_3 \cos \theta = 0, \quad (5)$$

and about C gives

$$T (c' - a) - T_M c' - T_4 b = 0 \quad . \quad (6)$$

From equation (4)

$$T_3 = \frac{Ta}{b \cos \theta + c' \sin \theta} = \frac{Ta}{b} \left(\frac{1}{\cos \theta + \frac{c'}{b} \sin \theta} \right) \quad . \quad (7)$$

Resolving vertically

$$\begin{aligned} T_M &= T - T_3 \sin \theta \\ &= T - \frac{Ta}{b} \frac{1}{\cos \theta + \frac{c'}{b} \sin \theta} \\ &= T \left(1 - \frac{a}{b \cos \theta + c' \sin \theta} \right) \quad . \quad (8) \end{aligned}$$

Resolving horizontally

$$\begin{aligned} T_4 &= - T_3 \cos \theta \\ &= - \frac{Ta}{b} \left(\frac{\cos \theta}{\cos \theta + \frac{c'}{b} \sin \theta} \right) \\ &= - \frac{Ta}{b} \left(\frac{1}{1 + \frac{c'}{b} \tan \theta} \right) \quad . \quad (9) \end{aligned}$$

Equations (7), (8) and (9) have been reduced to a form in which they are composed of the thrusts when aligned multiplied by a factor caused by misalignment.

If we take a typical instance where the ratio of $b:c':a$ is 100:40:1 we can evaluate the errors caused by different amounts of strut misalignment and these are given in Table 3. It can be seen that an error of up to 3° would be tolerable, but in practice the alignment attained is much better.

APPENDIX 4

Analysis of data from thrust alignment records

For the purpose of analysis the thrust stand is considered to contain three orthogonal axes formed by the intersection of three orthogonal planes (O , H and R) as in Fig. 11, and each containing the axes of struts as follows:

- O plane - containing axes of f , e and d
- R plane - containing axes of i , h and d
- H plane - containing axes of h , e and g .

The geometric axis of the motor is vertical and is coincident with the axis of the strut d . The motor thrust is normally in such a direction as to put strut d into compression. The force in all struts is denoted by the letter identifying the strut and tensile forces in all struts are considered positive with the exception of d in which compressive forces are positive. This convention arises from the method of calibration of the struts and reduces the probability of error if it is retained throughout the analysis.

Consider a thrust vector T acting in a completely general direction through the system passing through a point K in the O plane and E in the R plane. This force can be resolved at K into three forces, T_O , T_R and T_H acting in the three planes. T_O and T_R make small angles of α and β respectively with the vertical through K . m and L are the distances of K and E respectively above the H plane and distances in the upward direction are considered positive. b is the distance between the f and e or i and h struts and c' is the distance between the g and e struts.

Resolving the forces in each plane we have in the O plane

$$T_O \sin \alpha = f + e + g ,$$

$$T_O \cos \alpha = d .$$

Therefore

$$T_O = \sqrt{(f + g + e)^2 + d^2}$$

and

$$\sin \alpha = \frac{f + e + g}{\sqrt{(f + e + g)^2 + d^2}} \approx \frac{f + e}{d} ,$$

as $(f + e + g)^2 : d^2$ is usually about $1:10^5$ and g is small. Moving T_0 along its line of action and resolving where it intersects the vertical axis of d we have, taking moments about the axis of the h strut,

$$L T_0 \sin \alpha = bf$$

or

$$L = \frac{bf}{T_0 \sin \alpha} = \frac{bf}{f + e + g} \approx \frac{bf}{f + e} .$$

Similarly in the R plane

$$T_R \sin \beta = i + h ,$$

$$T_R \cos \beta = d .$$

Therefore

$$T_R = \sqrt{(i + h)^2 + d^2}$$

and

$$\sin \beta = \frac{i + h}{\sqrt{(i + h)^2 + d^2}} \approx \frac{i + h}{d}$$

as before.

Taking moments in the R plane about the axis of the e strut gives

$$m T_R \sin \beta = ib ,$$

so

$$m = \frac{ib}{T_R \sin \beta} = \frac{ib}{i + h} .$$

Resolution of torque

There may still remain a torque which could be obtained simply from

$$\text{torque} = c' g \quad .$$

The difficulty in practice is that direct measurement of the torque is not practicable with the small side forces involved. Let us consider a motor of 5000 N (1130 lbf) axial thrust, when the maximum torque is likely to be 20 N (4 lbf) at a distance of 2.5 mm (0.1 inch) from the axis. In a practical rig the distance c' is likely to be about 150 mm (6 inches), so that the force to be measured in g is 0.33 N (0.07 lbf) maximum. If g is displaced vertically the moment arm c' could be reduced to 2.5 mm (0.1 inch) but even to attain 1% accuracy it would have to be positioned to ± 0.025 mm (0.001 inch) in relation to the 0 plane. With this configuration the stiffness in torque, and hence the natural frequency, would be low.

The solution adopted is to leave strut g at about 150 mm (6 inches) from strut e but not to measure the force in it. As we have seen, the force in e does not differ by more than 2% from the total in e and g so that the force in g can be ignored. It can be shown that the torque is given by $n T_R \sin \beta$, but

$$n = (m - L) \tan \alpha$$

and

$$\tan \alpha = \frac{\sin \alpha}{\cos \alpha} = \frac{f + e + g}{d} \quad .$$

Therefore

$$\begin{aligned} \text{torque} &= \frac{(m - L) (f + e + g) (i + h)}{d} \\ &= \frac{(m - L) (f + e) (i + h)}{d} \end{aligned}$$

as g is small.

The value of the original thrust vector T is given by

$$T = \sqrt{(f + e)^2 + d^2 + (i + h)^2}$$

when g is ignored.

In practice the difference between T and d is negligible.

The "miss distance" of the thrust vector from the axis can be calculated at any plane at right angles to the axis as follows.

Let the distance from the origin to the plane be P , then

$$\text{miss distance in the O plane, } O' = (L - P) \tan \alpha = \left(\frac{bf}{f + e} - P \right) \frac{f + e + g}{d}$$

$$\text{miss distance in the R plane, } R' = (m - P) \tan \beta = \left(\frac{ib}{i + h} - P \right) \frac{i + h}{d}$$

$$\therefore \text{ total miss distance} = \sqrt{\left(\left[\frac{bf}{f + e} - P \right] \frac{f + e + g}{d} \right)^2 + \left(\left[\frac{ib}{i + h} - P \right] \frac{i + h}{d} \right)^2}$$

The angle, A , about the axis between the left hand struts, as origin, and the line joining the axis to the point where the vector passes through the plane at P can be calculated as follows:

$$\tan A = \frac{O'}{R'} = \frac{\left(\frac{bf}{f + e} - P \right) \frac{f + e + g}{d}}{\left(\frac{ib}{i + h} - P \right) \frac{i + h}{d}}$$

The quadrant is given by

sign of O'	- ve	- ve	+ ve	+ ve
sign of R'	- ve	+ ve	- ve	+ ve
quadrant	1st	2nd	3rd	4th

APPENDIX 5

Design of hydraulic clamp

The arrangement of one set of clamps is shown in Fig. 16. Pressure is initially applied to the pistons so that a sufficient balanced load is applied to compress any air bubbles in the system and take up any slack.

Assume an impulsive load F on the piston, diameter D , generating a pressure difference of $\frac{4F}{\pi D^2}$ between the opposed pistons. Let this operate for a period t during which the permissible displacement is d (this is some small fraction of the rig displacement at maximum load). The volume of fluid displaced is $\frac{\pi D^2 d}{4}$ and the volume flow rate is $\frac{\pi D^2 d}{4 \cdot t}$.

Let the bore of the restriction be $2r$ and the fluid viscosity η . The length of tubing required, L , is $\frac{2 r^4 F t}{\pi D^4 d}$.

A similar calculation gives the force required to move the pistons clear of the rig in the time available after the impulsive load, the flow in this case being through a pipe $L/2$ in length. Direct venting of the cylinders is undesirable, as separate vents are required for each cylinder and if these do not operate simultaneously large loads may be applied to the rig.

APPENDIX 6

Analysis of ballistic pendulum

Assume a pendulum of mass M and effective length L . Let it move from rest under the action of a force F through an angle α so that its centre of mass moves along an arc by a distance s . Let its velocity at any instant be v .

CASE 1

Let the force F be impulsive, so that any movement of the mass during the application of the force is negligible and the initial velocity after the impulse is v_i .

We have

$$M \frac{d^2 s}{dt^2} = -Mg \sin \alpha$$

or

$$Mv \frac{dv}{ds} = -Mg \sin \frac{s}{L}$$

$$\therefore M \int_{v_i}^0 v dv = -Mg \int_0^{s_2} \sin \frac{s}{L} ds \quad \text{where } s_2 \text{ is the maximum displacement}$$

$$M \left[\frac{v^2}{2} \right]_{v_i}^0 = -Mg \left[-L \cos \frac{s}{L} \right]_0^{s_2}$$

$$\frac{-Mv_i^2}{2} = MgL \frac{\cos s_2}{L} - mgL = MgL \left(\cos \frac{s_2}{L} - 1 \right)$$

$$\therefore \int F dt = Mv_i = M \sqrt{2gL \left(1 - \cos \frac{s_2}{L} \right)}$$

It is necessary to know M , g and L and to measure s_2

CASE 2

Let the force F be applied instantaneously and remain at a constant value until removed instantaneously after an interval t during which the mass moves a distance s , and acquires a velocity v .

$$M \frac{d^2 s}{dt^2} = F - Mg \sin \alpha$$

or $Mv \frac{dv}{ds} = F - Mg \sin \frac{s}{L}$

$$\therefore M \int_0^{v_i} v \, dv = F \int_0^{s_1} ds - Mg \int_0^{s_1} \sin \frac{s}{L} ds$$

$$M \left[\frac{v^2}{2} \right]_0^{v_i} = F \left[s \right]_0^{s_1} - Mg \left[-L \cos \frac{s}{L} \right]_0^{s_1}$$

$$F = \frac{Mv_i^2}{2s_1} + \frac{MgL}{s_1} (1 - \cos \frac{s_1}{L})$$

$$\therefore \int F dt = \int \left[\frac{Mv_i^2}{2s_1} + \frac{MgL}{s_1} (1 - \cos \frac{s_1}{L}) \right] dt \dots\dots\dots (1)$$

Measurement of v_i , s_1 and t would enable $\int F dt$ to be evaluated but accurate velocity measurement is not easy and it is usual to measure the maximum swing of the mass.

After the force ceases we have, as in case 1,

$$M \int_{v_i}^0 v \, dv = -Mg \int_{s_1}^{s_2} \sin \frac{s}{L} ds \quad \text{where } s_2 \text{ is the displacement of the mass at full swing.}$$

Integrating, $M \left[\frac{v^2}{2} \right]_{v_i}^0 = Mg \left[L \cos \frac{s}{L} \right]_{s_1}^{s_2} .$

Evaluating and dividing by s_1

$$\frac{-Mv_i^2}{2s_1} = \frac{MgL}{s_1} (\cos \frac{s_2}{L} - \cos \frac{s_1}{L}) .$$

Substituting in (1) gives

$$\int F dt = \int \frac{MgL}{s} (1 - \cos \frac{s_2}{L}) dt \quad .$$

It is now necessary to measure s_1 , s_2 and t to evaluate $\int F dt$.

CASE 3

The force F varies with time but conditions are otherwise as for case 2.

$$M \frac{dv}{dt} = F - Mg \sin \frac{s}{L}$$

$$\therefore \int_0^t F dt = M \int_0^{v_i} dv + Mg \int_0^{s_1} \sin \frac{s}{L} dt$$

$$\int_0^t F dt = Mv_i + Mg \int_0^{s_1} \sin \frac{s}{L} dt \quad .$$

Mv_i may be evaluated as in case 2 to give

$$\int_0^t F dt = M \sqrt{2g L (\cos \frac{s_1}{L} - \cos \frac{s_2}{L})} + Mg \int_0^{s_1} \sin \frac{s}{L} dt \quad .$$

In addition to s_1 and s_2 it is now necessary to know how s varies with t from rest to s_1 .

APPENDIX 7

Decelerating device (initial design)

The device consists of a piston and cylinder filled with hydraulic oil and pressurised from a nitrogen filled reservoir. The piston is held at the outer limit of its travel by a lip on the cylinder. When the mass contacts the piston after the motor has fired, it is brought to rest by the force applied by the piston. If the reservoir is large enough the pressure on the piston changes only slightly during the stroke and the measured force does not increase excessively. The measuring system can thus work in the most accurate part of its range.

To prevent acceleration of the mass in the reverse direction after it is brought to rest a restrictor valve comes into operation when the flow between cylinder and reservoir reverses. The size of the restriction is chosen so that the measured force of the load cell is less than 0.1% of that during the forward stroke of the piston. This ensures that any small error in timing the thrust integration results in a negligible error in total impulse, and the mass is returned gently to its starting point.

Typical sizes and operating values can be calculated using the example in the main body of the text of a force, R , of 4000 N acting for 250 ms, resulting from a motor impulse of 1000 Ns. This requires a pressure of $\frac{4000}{a}$ where a is the piston area. Let $d = 0.1$ m.

$$\text{Pressure required in cylinder is } \frac{4000.4}{\pi \cdot 10^{-2}} = 0.51 \text{ MNm}^{-2}.$$

$$\text{Velocity of the block after the impulse is } v = \frac{I}{M} = 1 \text{ ms}^{-1}.$$

$$\text{This is brought to rest in a distance } s = \frac{v^2 M}{2R} = 0.125 \text{ m}.$$

$$\text{The volume of oil displaced} = \frac{\pi \cdot 10^{-2} \cdot 0.125}{4} = 0.00098 \text{ m}^3,$$

$$\therefore \text{ the flow rate is } \frac{0.00098}{0.25} = 0.00392 \text{ m}^3 \text{ sec}^{-1}.$$

If it is assumed that a pressure drop of 1% of the pressure in the reservoir is acceptable for flow through the connector from the cylinder to the reservoir, i.e. 5100 Nm^{-2} , the minimum radius of the connector, $r_i = \frac{Q \cdot 81 \eta}{\pi P}$

$$\begin{aligned} \text{where } Q &= \text{flow rate} &= 0.00392 \text{ m}^3 \text{ sec}^{-1} \\ l &= \text{length of connector} &= 10^{-3} \text{ m} \end{aligned}$$

η = viscosity of oil = 0.05 Pascal sec

P = pressure difference across connector = 5100 Nm⁻²

$$r_i^4 = \frac{0.00392 \cdot 8 \cdot 10^{-3} \cdot 0.05}{\pi \cdot 5100} \text{ m}^4$$

$$r_i = 3.145 \text{ mm} .$$

This is easily achieved, but allowance must be made for the pressure rise in the reservoir, which progressively reduces the stroke and the flow rate, depending on the size of reservoir which can be accommodated. In practice an initial gas volume of three times the oil displacement results in a pressure rise of up to 1.5 times the initial pressure. This permits sufficiently accurate impulse measurement.

Return flow must be restricted to 10^{-3} of the forward flow, so that the radius, r_2 , of the restrictor is given by

$$r_2^4 = \frac{0.00392 \cdot 10^{-3} \cdot 8 \cdot 10^{-3} \cdot 0.05}{\pi \cdot 510 \cdot 10^3} \text{ m}^4$$

$$r_2 = 0.177 \text{ mm} .$$

A hole of this size can be incorporated in a simple light flap valve which closes as the mass reverses direction.

APPENDIX 8

Examples of use of graphs giving dynamic response

Example 1

Problem

The initial pressure/time curve of a rocket motor approximates to a linear rise lasting 2.5 ms. It is required to measure this to an accuracy of $\pm 5\%$. The system is damped to 0.6 of critical. What must be the least natural frequency of the measuring system?

Method

Look along the 5% error line to the point where it intercepts the graph (Fig. 26) $h = 0.6$. This occurs at a value of $f_n t_{\max}$ of approximately 4.5. We are given that $t_{\max} = 0.0025$ sec, therefore

$$f_n = \frac{4.5}{0.0025} = 1800 \text{ Hz}.$$

The system must have a lowest natural frequency of 1800 Hz at which the maximum delay in the recording of any point on the rise time is 5% of 2.5 ms, i.e. 0.125 ms.

Example 2

Problem

Given the same conditions as in Example 1, but let the required accuracy be $\pm 1\%$. What must be the lowest natural frequency of the measuring system?

Method

As before, but using the 1% error line, $f_n t_{\max} = 22$ approximately therefore

$$f_n = \frac{22}{0.0025} = 9000 \text{ Hz}.$$

Example 3

Problem

A thrust stand has a resonant frequency of 400 Hz and the rise time of thrust is known to be 1 ms. What errors will be incurred in amplitude measurements and delay if damping is 0.3 of critical? The bandwidth of all other parts of the measuring system is greater than 400 Hz.

Method

400 Hz \times 0.001 sec gives a value of $f_n t_{\max}$ of 0.4. Find where this line intercepts the graph $h = 0.3$, i.e. 45%. 45% of 1 ms = 0.45 ms.

Check that error due to overswing will not be greater than 45%.

Maximum amplitude error will be 45%.

Maximum time error will be 0.45 ms.

NOTE

This error will affect only the initial rise. If the motor fired for 100 ms the error in total integral due to the rise time error would not exceed 0.5% and when compensated by the overswing would be negligible.

Example 4

Problem

The pressure in the motor of Example 1 is required to be measured to $\pm 0.5\%$ at all times. All other factors being the same, what is the necessary natural frequency of the measuring system?

Method

Proceed as for Example 1. Multiply $f_n t_{\max}$ by 10 (to convert from 5% to 0.5% error) and since t_{\max} is the same $f_n = 18000$ Hz. Timing error = 0.0125 ms.

Example 5

Problem

A motor with a thrust rise time of 3 ms is to be fired on a stand which when shock excited by a blow has a natural frequency of 400 Hz, and the ratio of successive oscillation amplitudes is 20:1. What are the worst amplitude and timing errors?

Method

From Fig. 29, damping ratio is 0.43

$$f_n t_{\max} \text{ is } 0.003 \times 400 = 1.2.$$

From Fig. 26, error lies between 17% and 19% (0.3 and 0.5 damping ratio curves), say 18%.

$$\text{Timing error} = \frac{3.18}{100} = 0.54 \text{ ms} \quad .$$

Overswing error is less than 6% (0.3 damping ratio curve) but could be as much as 25% if a step function were applied to the stand.

TABLE 1

Main thrust (lbf)	0	500	1000	1500	2000
Side strut No.	Interaction in side struts (lbf)				
1	0	0	0.17	0.14	-0.1
2	0	0.2	0.8	1.3	1.66
3	0	0.82	1.06	1.65	1.95
4	0	0.11	0.60	1.04	1.50

Interaction forces

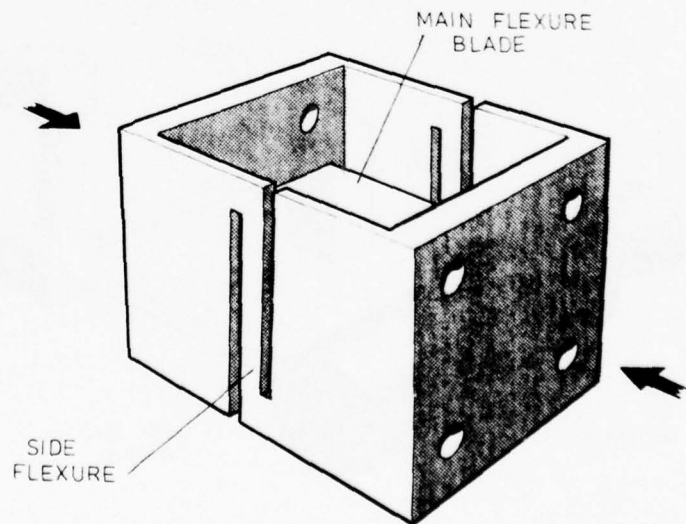
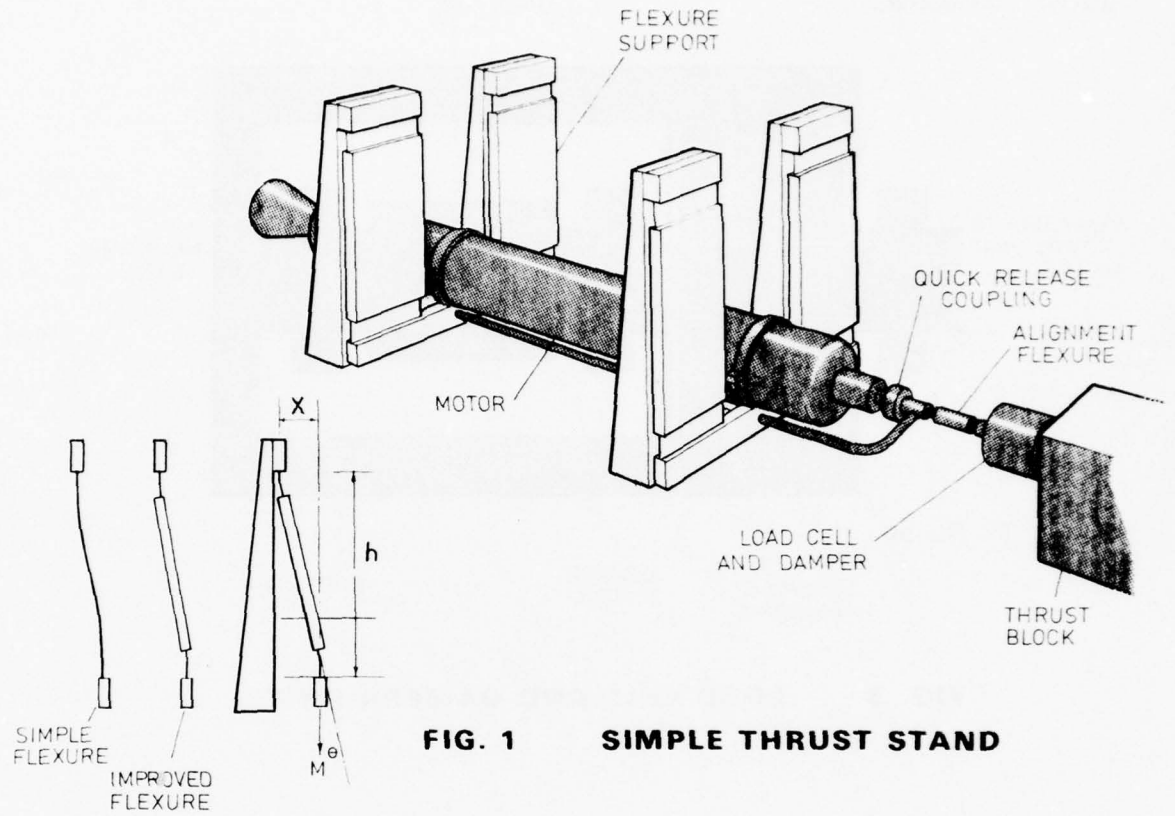
TABLE 2
Results of static loading of six component alignment rig

Load and position (see Fig. 13)		Cell No. (all loads in Newtons)											
		1			2			3			4		
		Expected	Measured		Expected	Measured		Expected	Measured		Expected	Measured	
2	(N)												
	50	0	-1.5	67	67	67	-73	-81	0	0	56	60	
	95	0	-0.5	127	127	127	-143	-144	0	1	116	122	
3	300	0	-0.5	400	402	402	-436	-431	0	3.75	336	347	
	50	0	0	0	2	2	-39	-41	0	0	89	90	
	100	0	0	0	4	4	-79	-81	0	0	179	183	
4	300	0	0	0	8.6	8.6	-236	-248	0	0	536	547	
	50	0	0	-67	-65	-65	-6	-10	0	0	122	122	
	100	0	0	-127	-129	-129	-16	-20.6	0	-0.7	243	243	
6	300	0	0	-400	-385	-385	-36	-60	0	-0.7	736	733	
	180	0	0	0	4.4	4.4	-173	-178	0	0	353	346	
7	45	0	0	0	1	1	-66	-66	0	0	111	111	
	90	0	0	0	0	0	-132	-133	0	0	222	223	
	135	0	0	0	0	0	-197	-201	0	0	332	335	

TABLE 3

Errors due to strut misalignment

Angular displacement of upper strut (T_3) θ degrees	Ratio of measured value of force in struts with respect to true value of unity		
	T_3	T_4	T_M
0	1	1	1
18'	0.9987	0.9987	
30'	0.9978	0.9978	
1°	0.9958	0.9956	
2°	0.9920	0.9913	
3°	0.9883	0.9869	0.9995



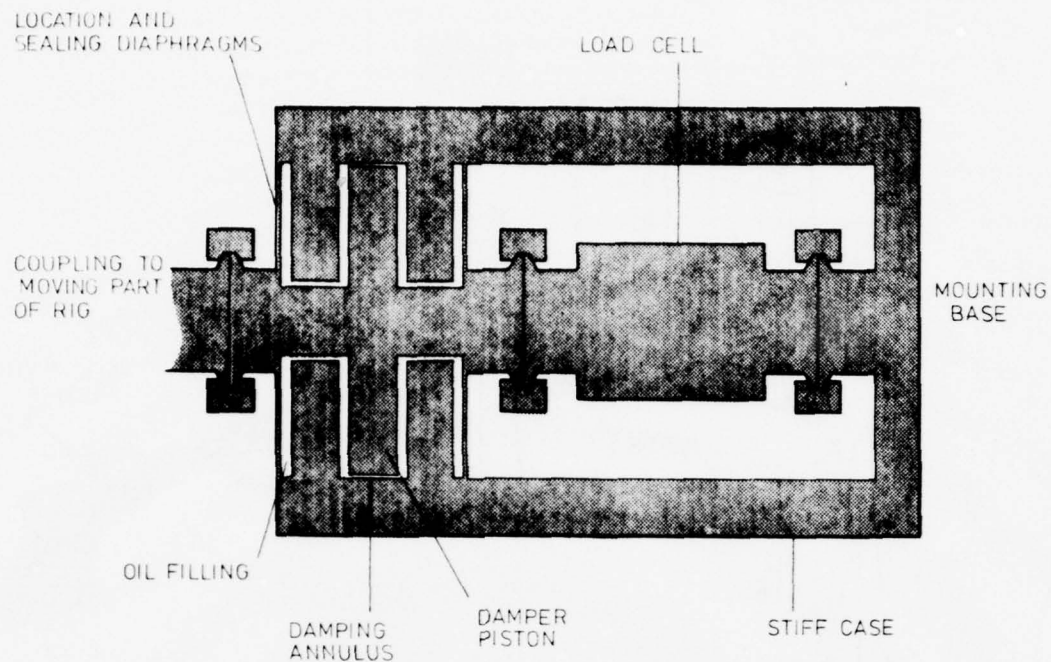


FIG. 3 LOAD CELL AND DAMPER UNIT

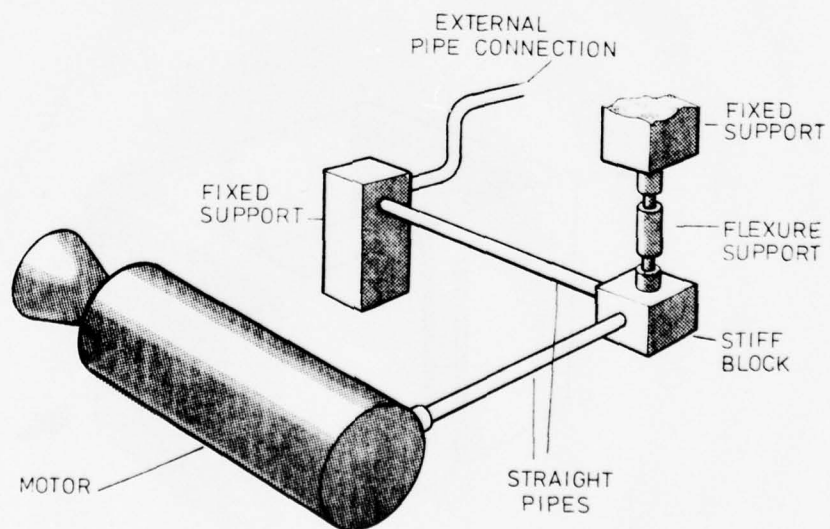


FIG. 4 FLUID FEED TO MOTOR

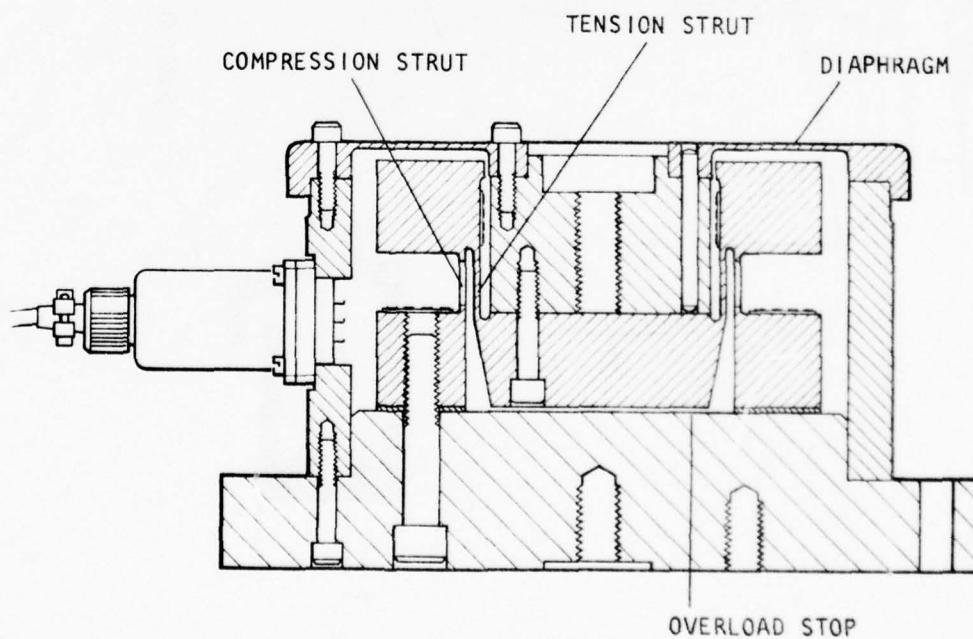
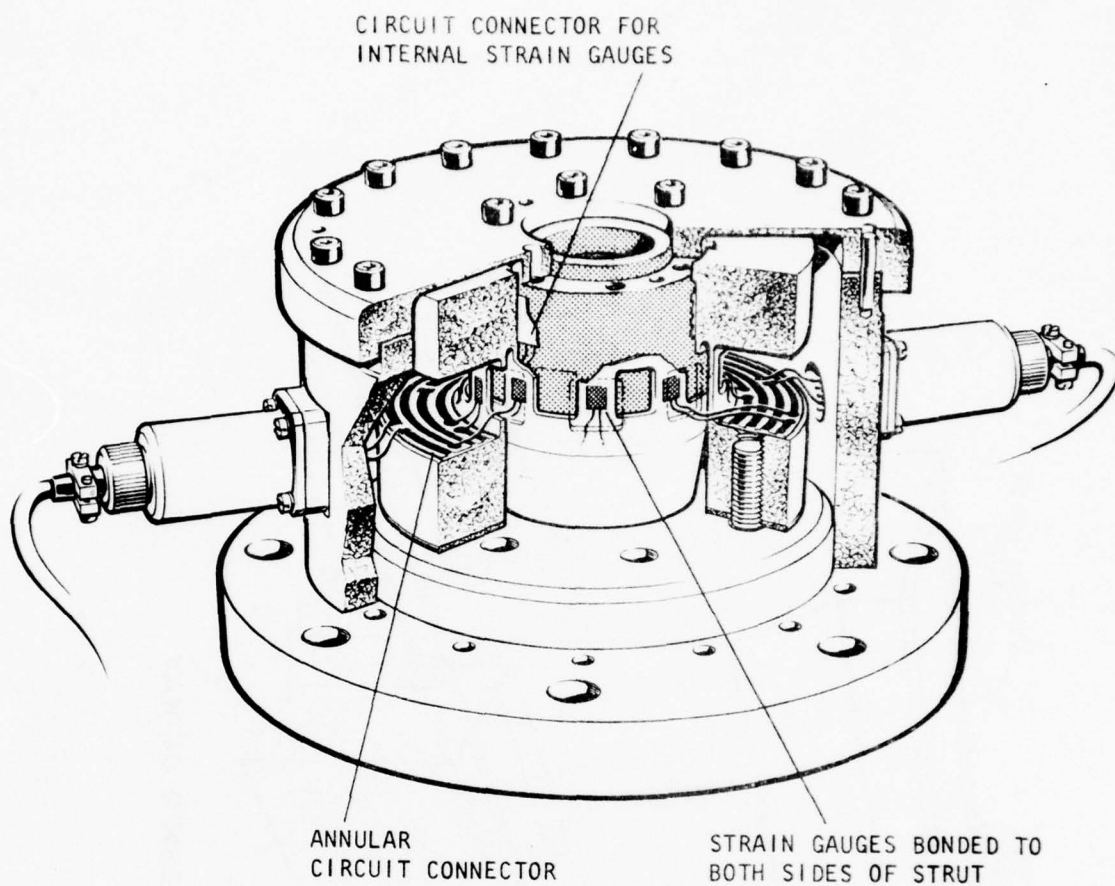


FIG. 5 PERME LOAD CELL

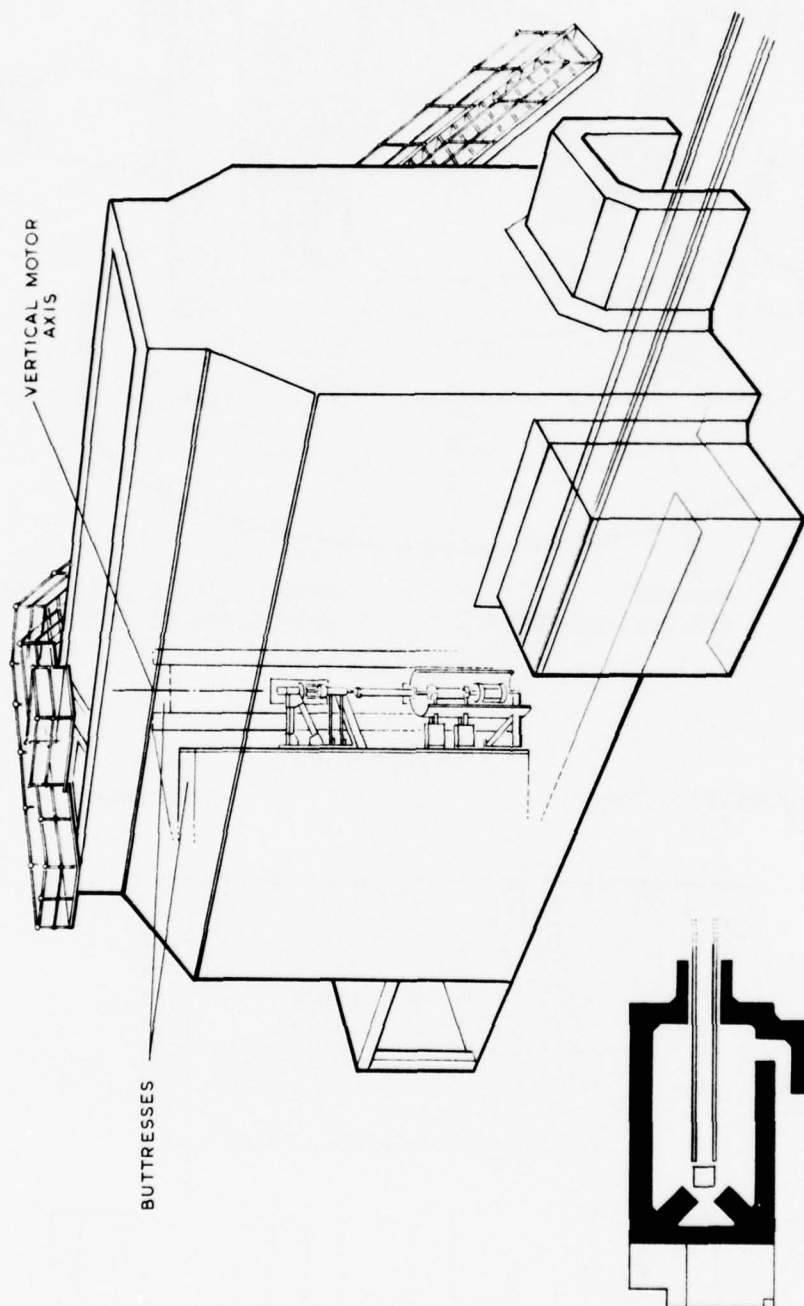


FIG. 6 DESIGN OF BAY

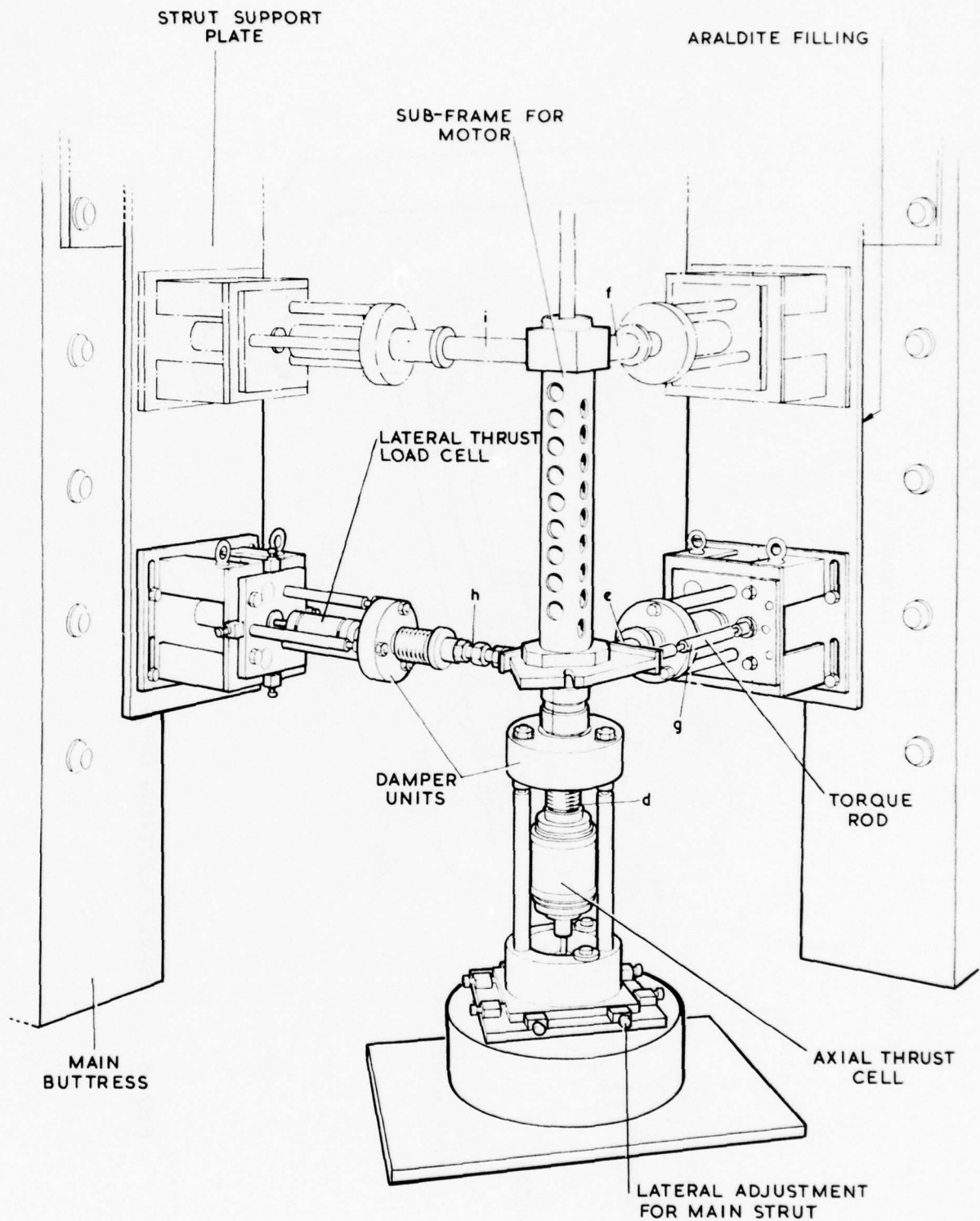


FIG. 7 VERTICAL THRUST ALIGNMENT ASSEMBLY

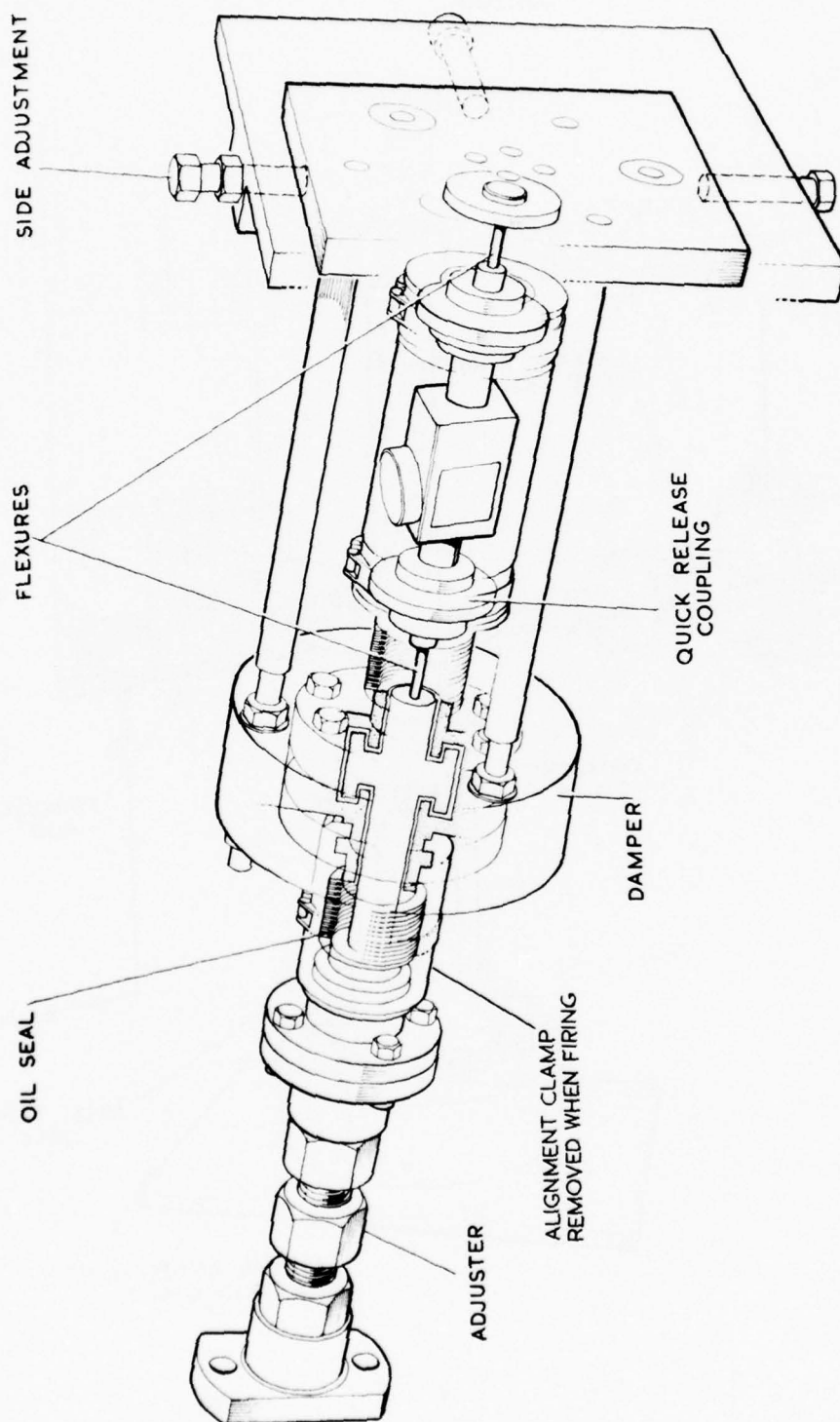


FIG. 8 CONSTRUCTION OF A STRUT

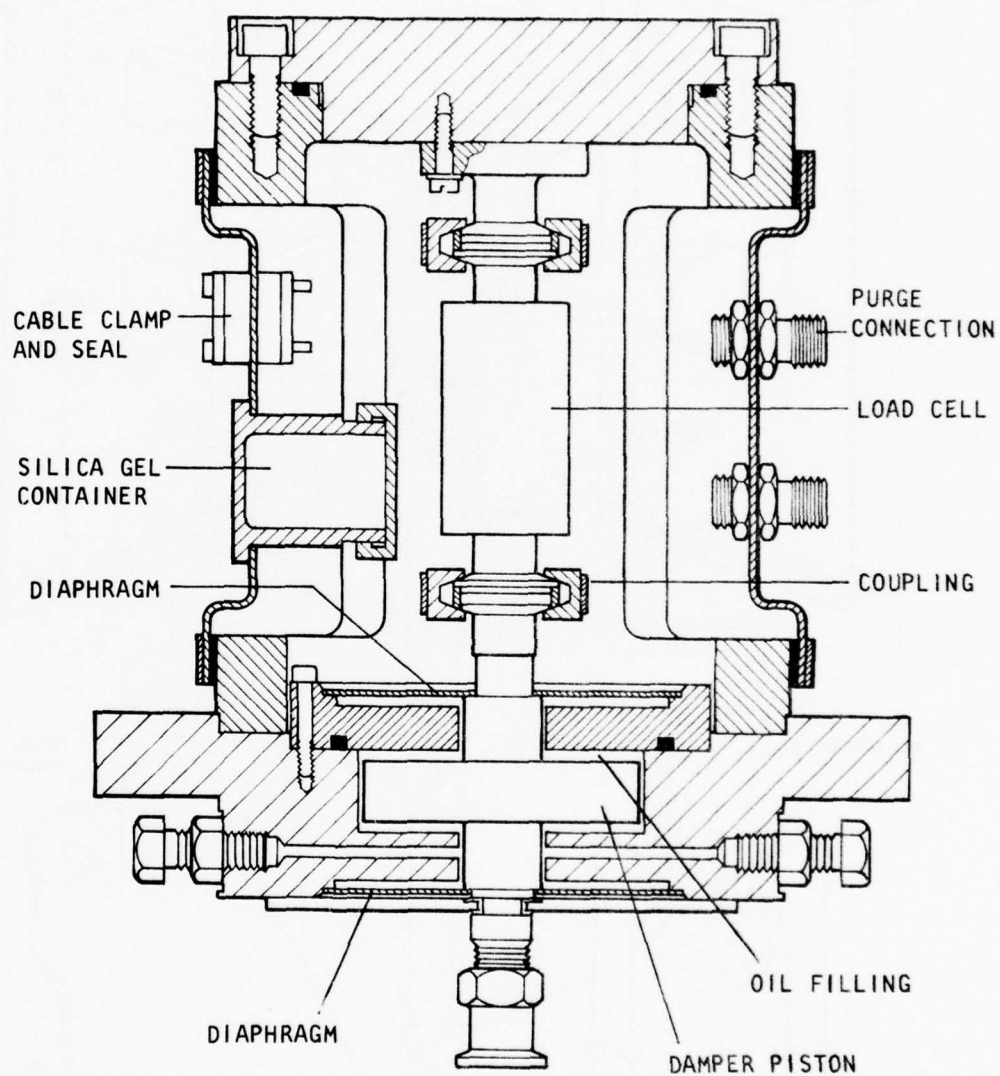


FIG. 9 LOAD CELL / DAMPER UNIT

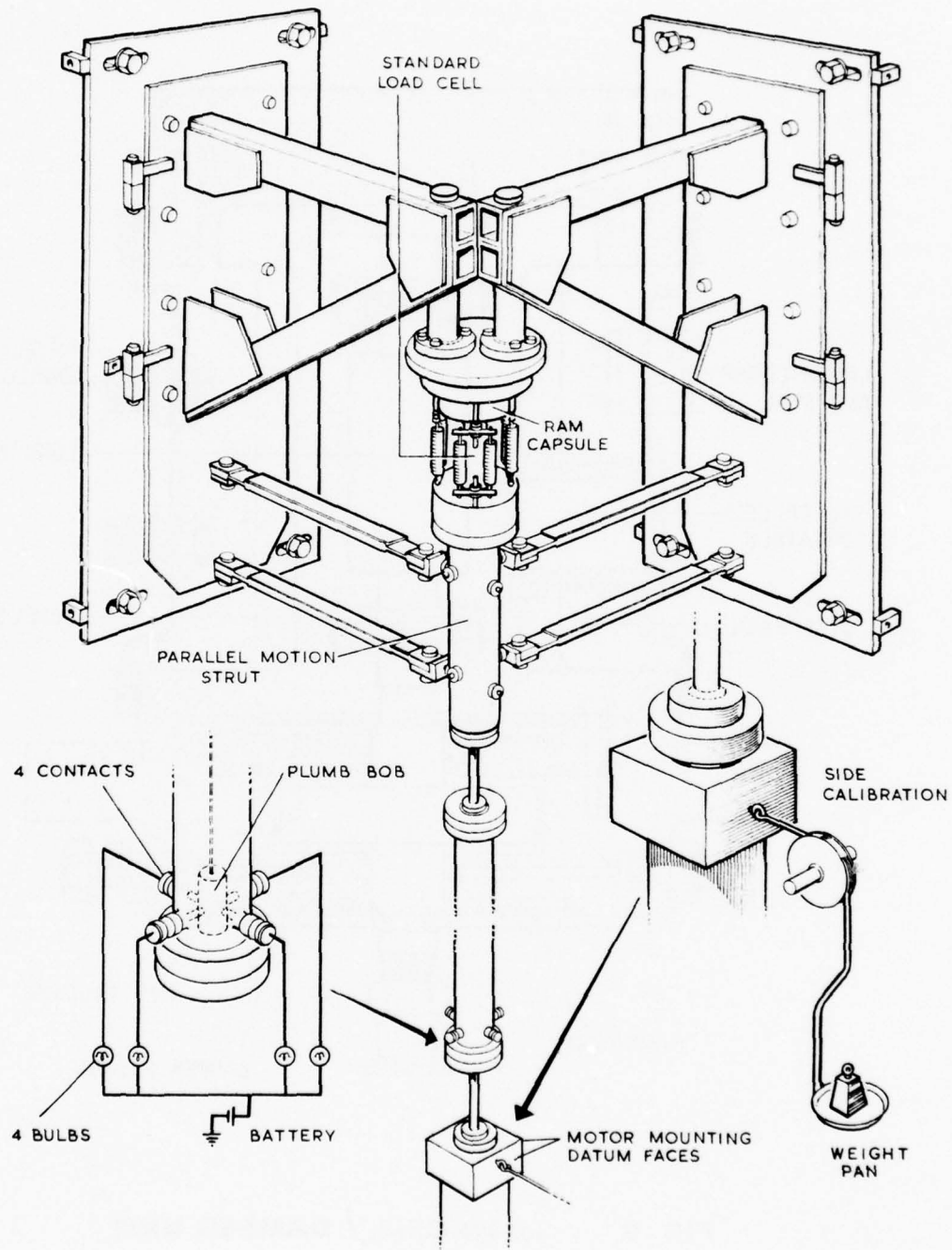


FIG. 10 CALIBRATION ASSEMBLY

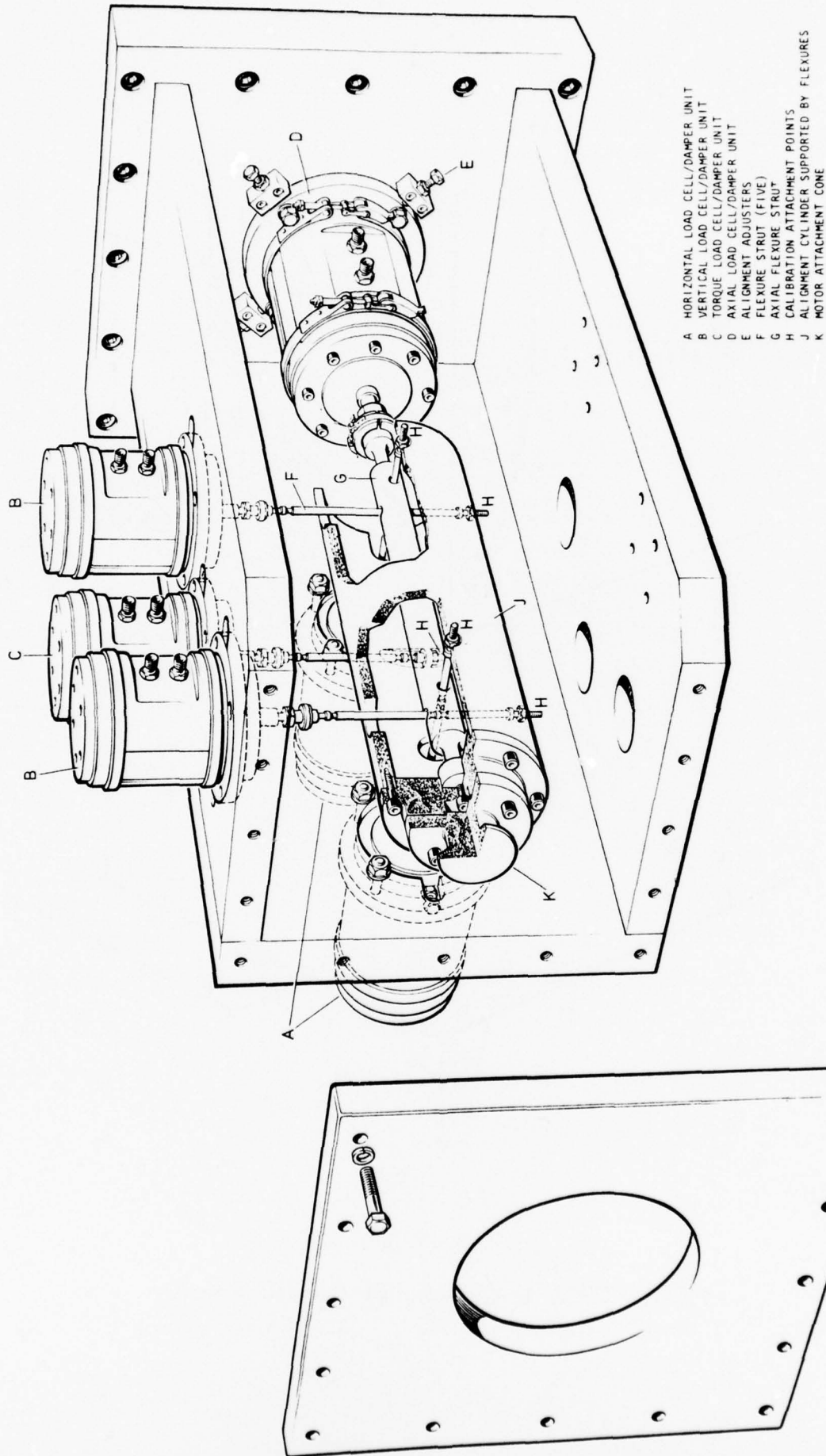


FIG. 12 HORIZONTAL THRUST ALIGNMENT ASSEMBLY

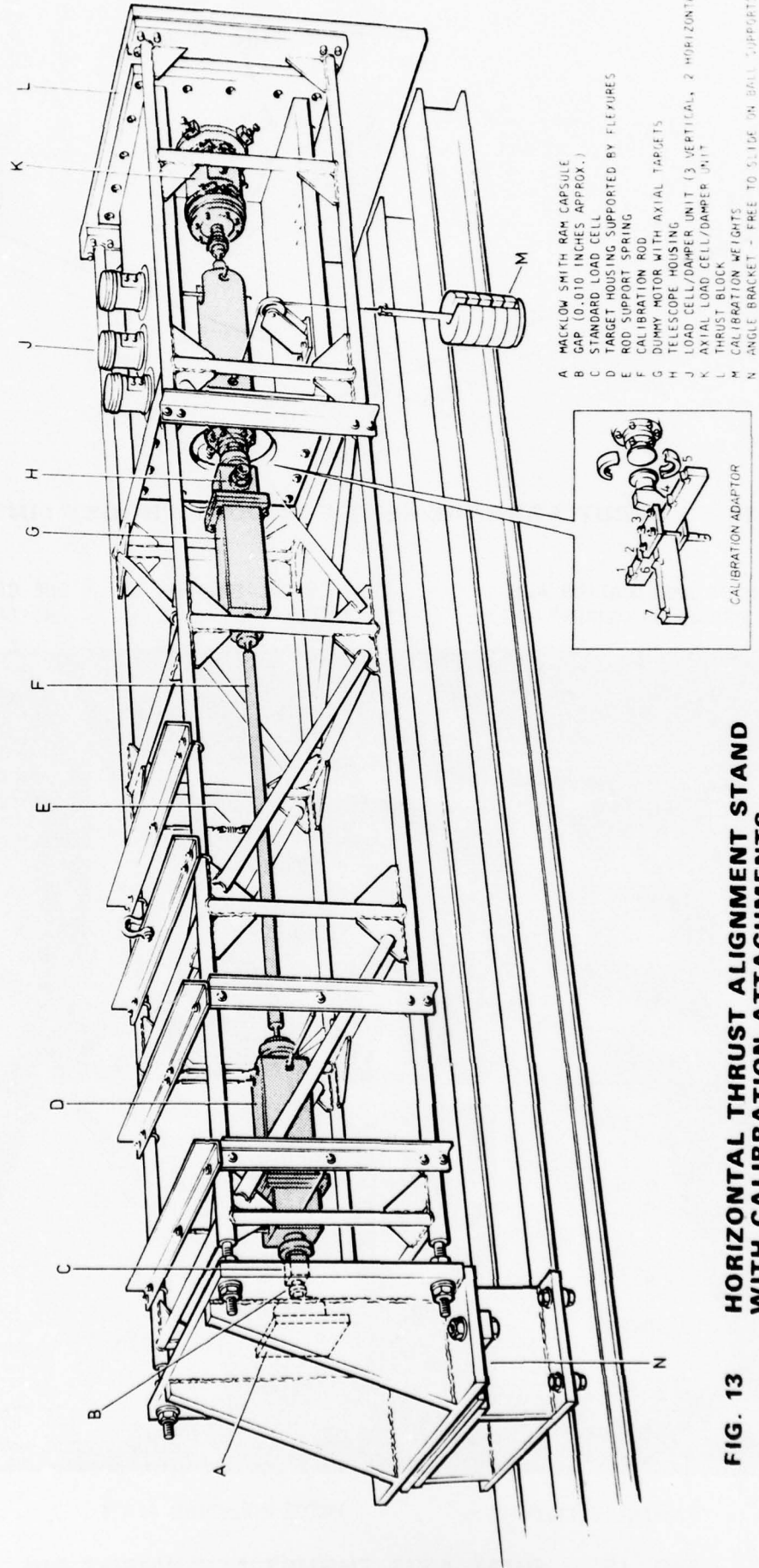
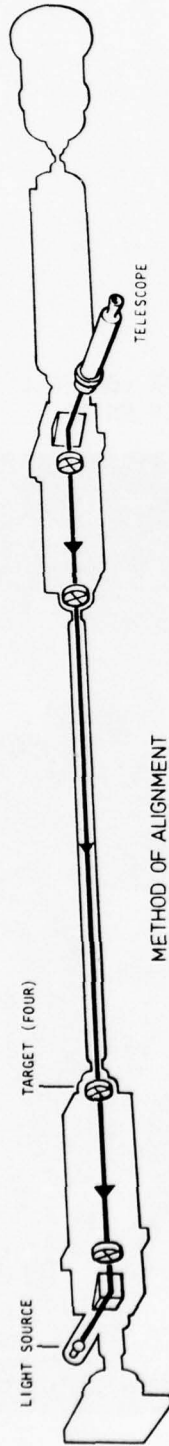


FIG. 13 HORIZONTAL THRUST ALIGNMENT STAND
WITH CALIBRATION ATTACHMENTS

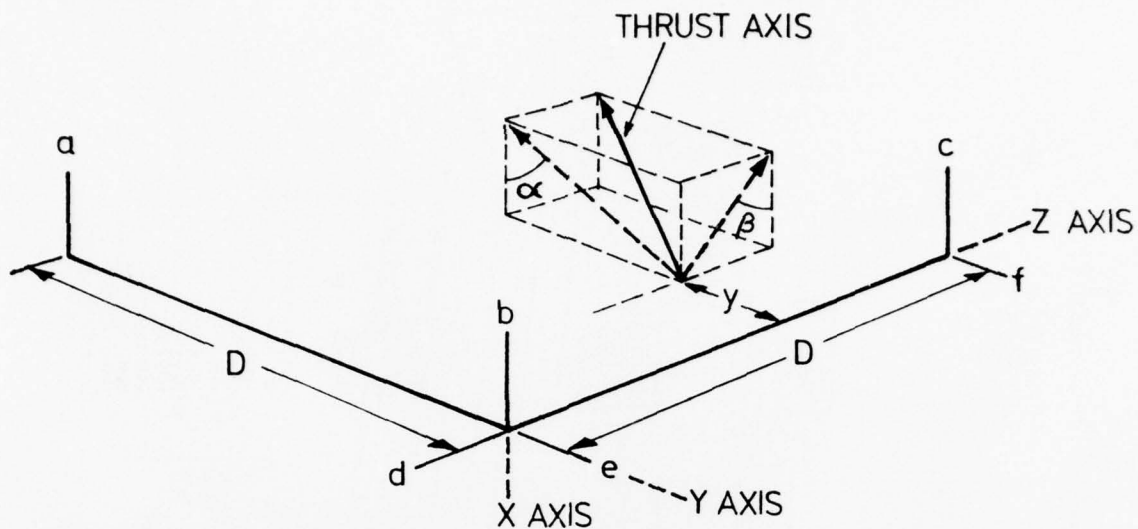


FIG. 14 STRUT ARRANGEMENT FOR DUAL THRUST LINES

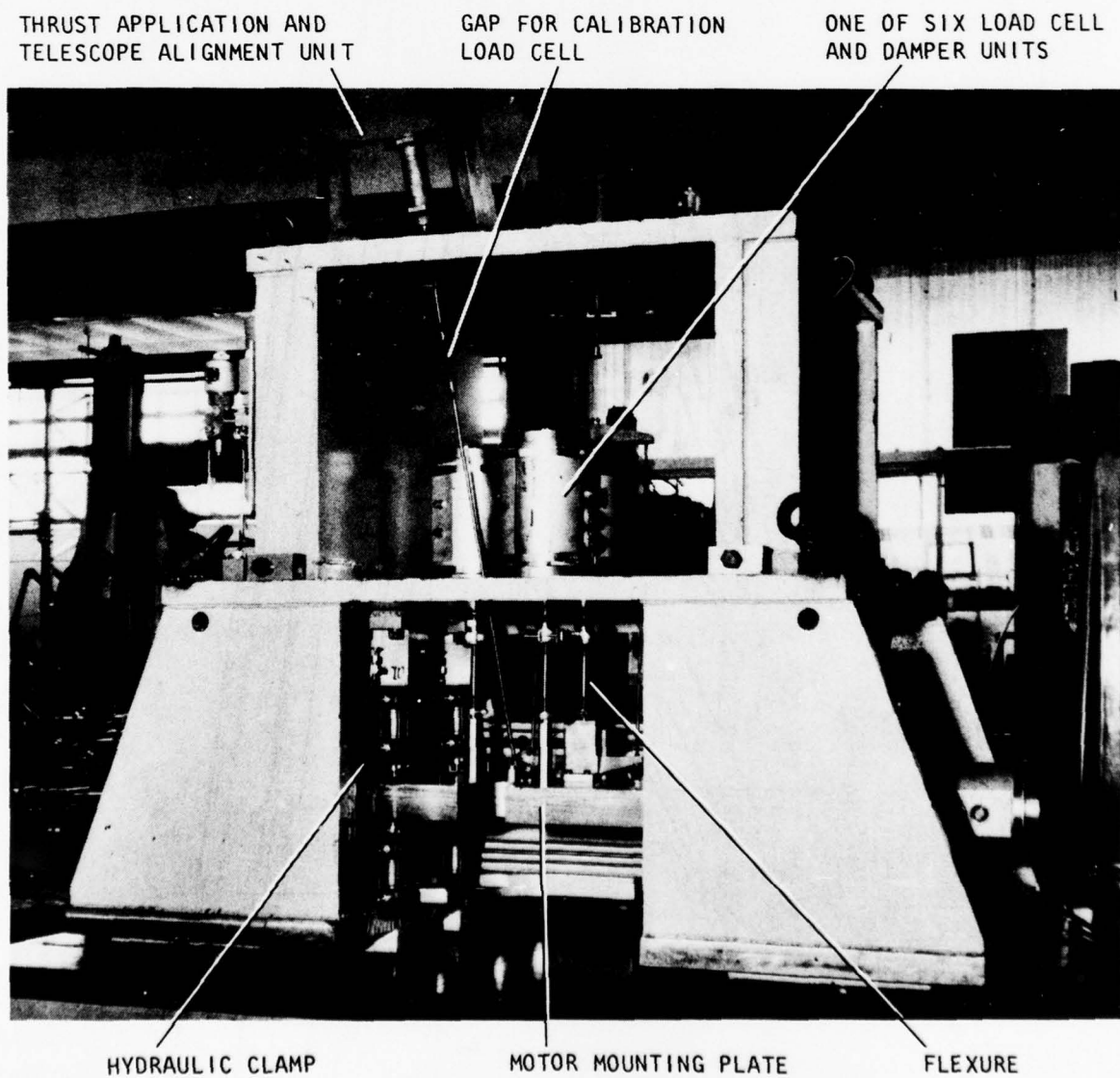


FIG. 15 DUAL AXIS THRUST ALIGNMENT RIG

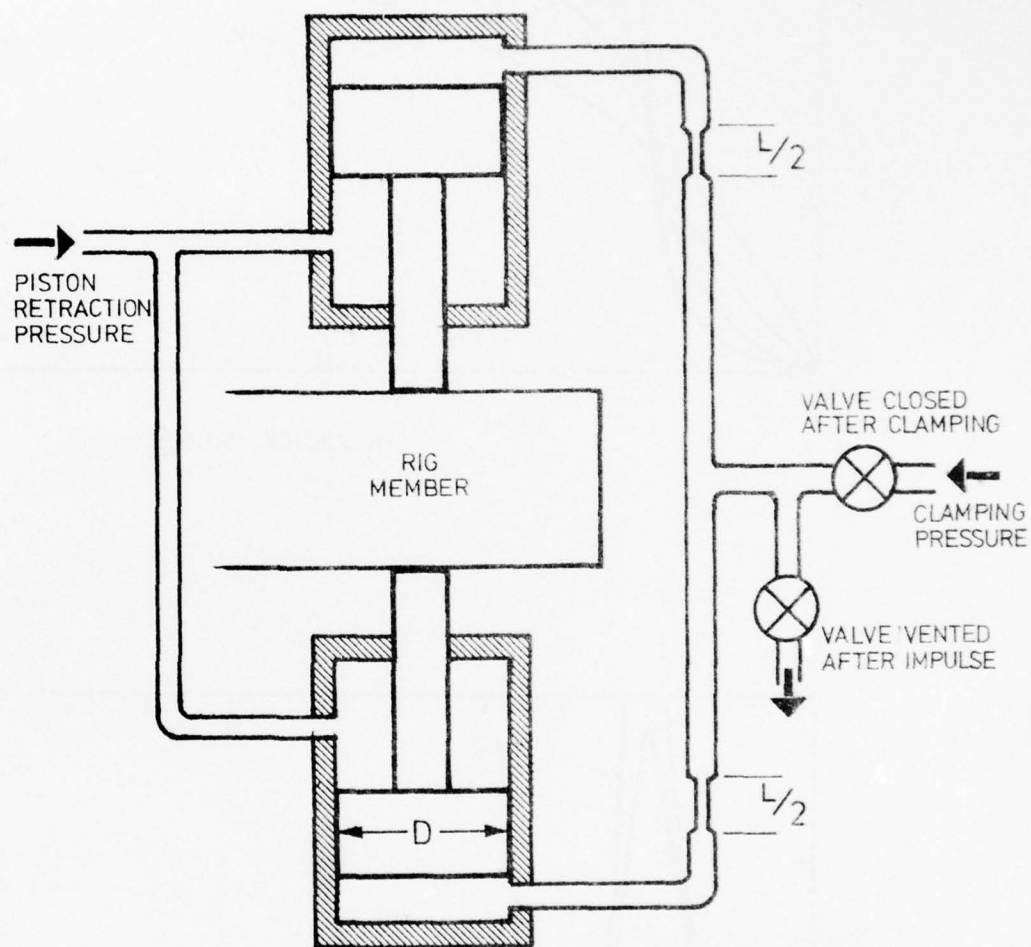


FIG. 16 HYDRAULIC CLAMPS

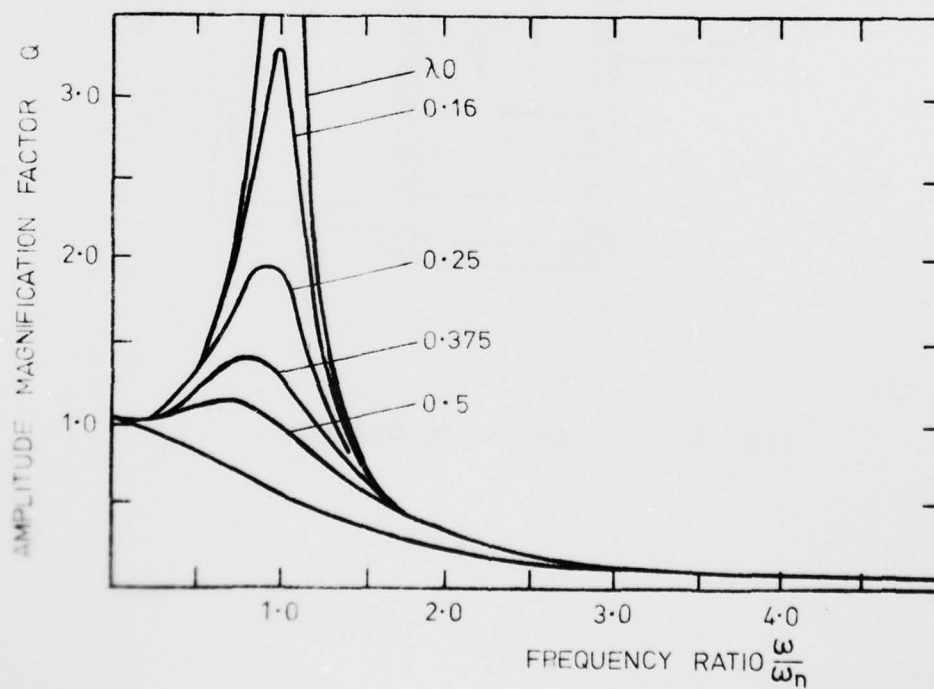
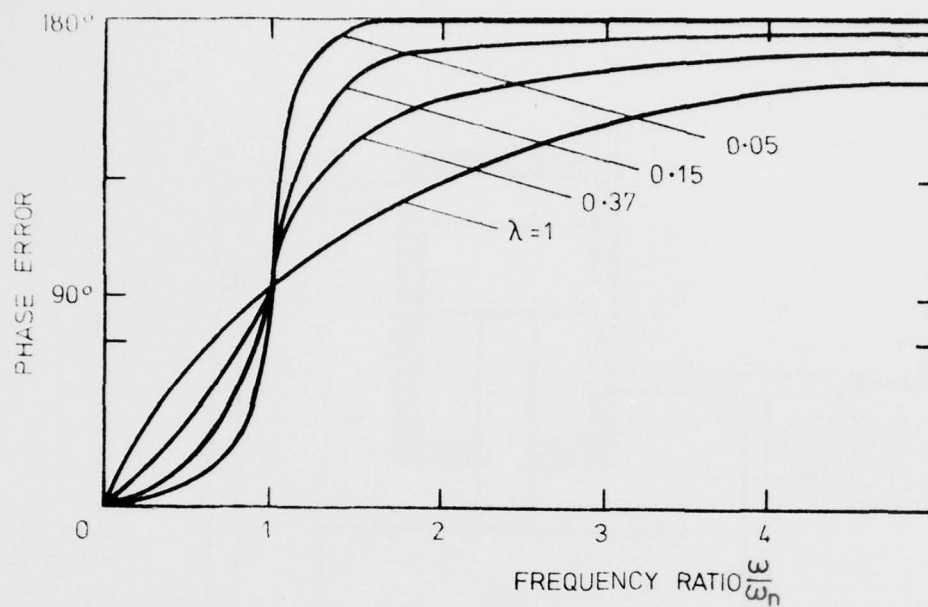


FIG. 17 PHASE AND AMPLITUDE ERRORS
IN DAMPED RESONANT SYSTEM

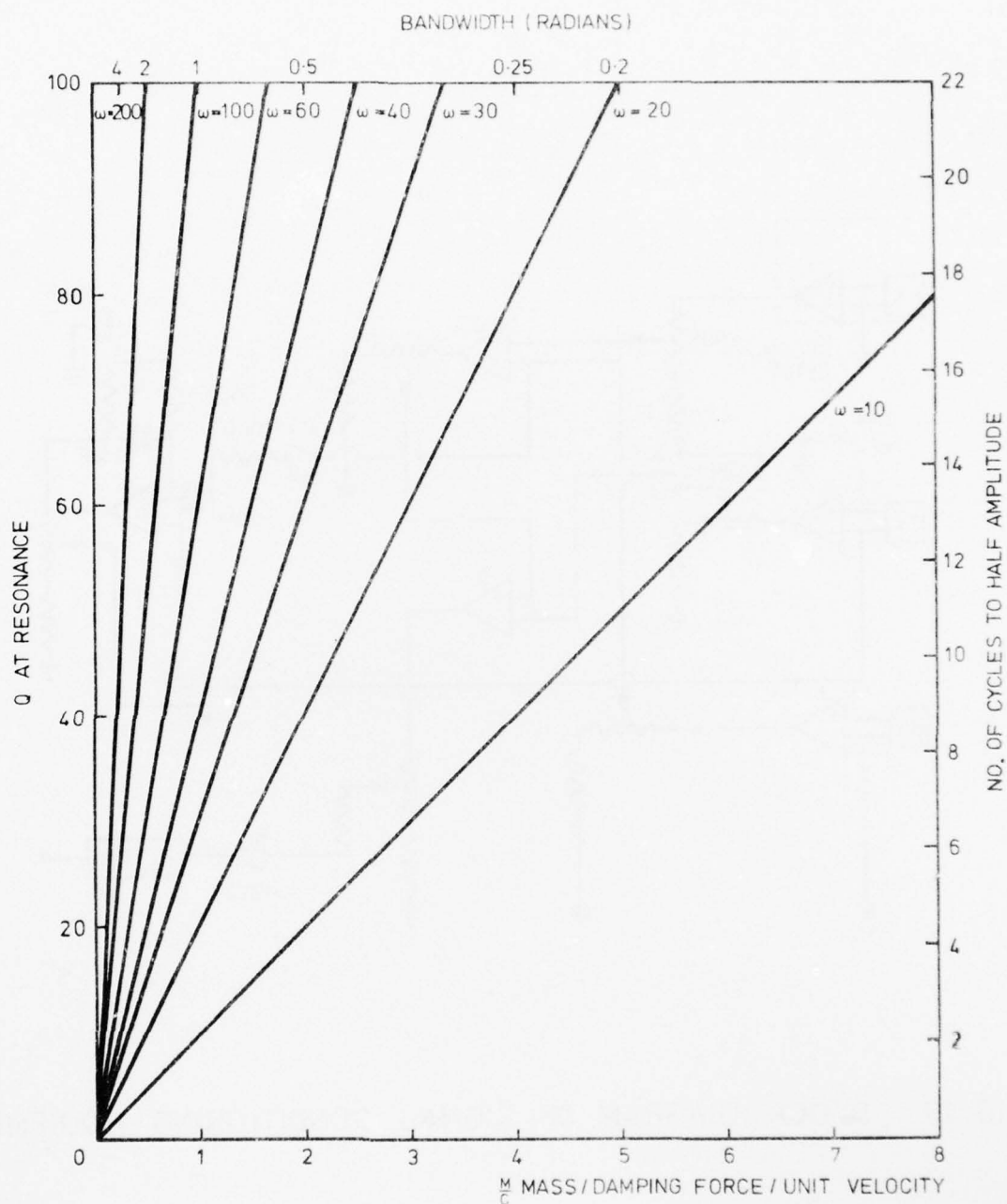


FIG. 18 GRAPHS RELATING Q , BANDWIDTH, NUMBER OF CYCLES TO HALF AMPLITUDE AND MASS PER DAMPING FORCE AT UNIT VELOCITY

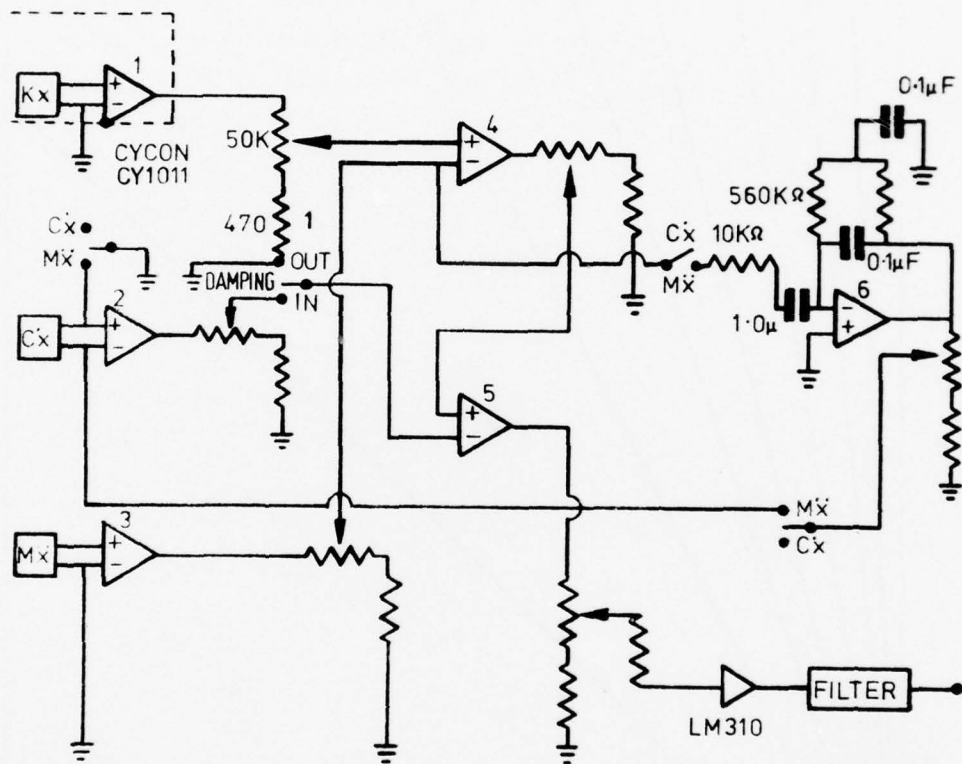


FIG. 19 BLOCK DIAGRAM OF SIGNAL CONDITIONING EQUIPMENT

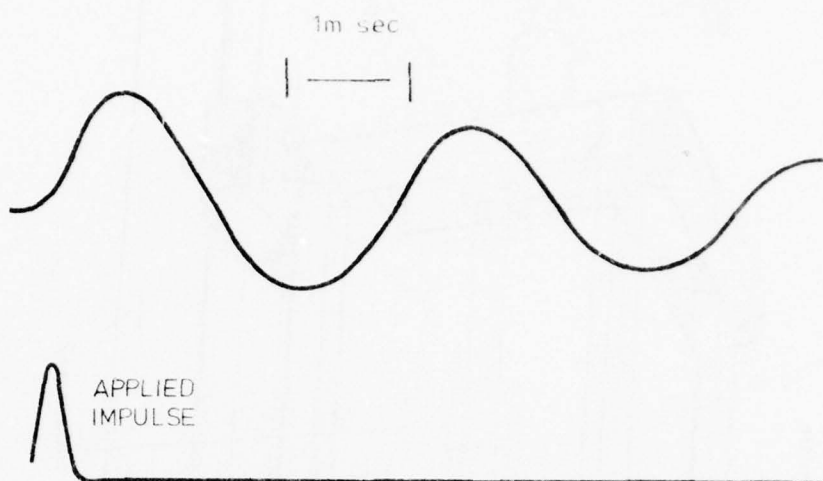


FIG. 20 UNCOMPENSATED REPONSE OF THRUST RIG

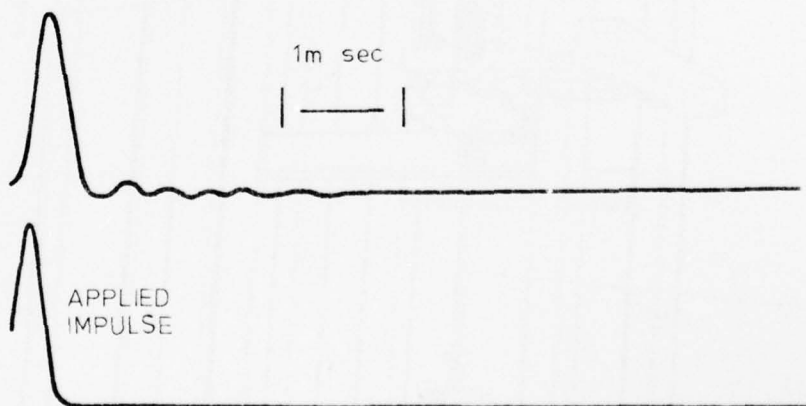


FIG. 21 COMPENSATED REPONSE OF THRUST RIG

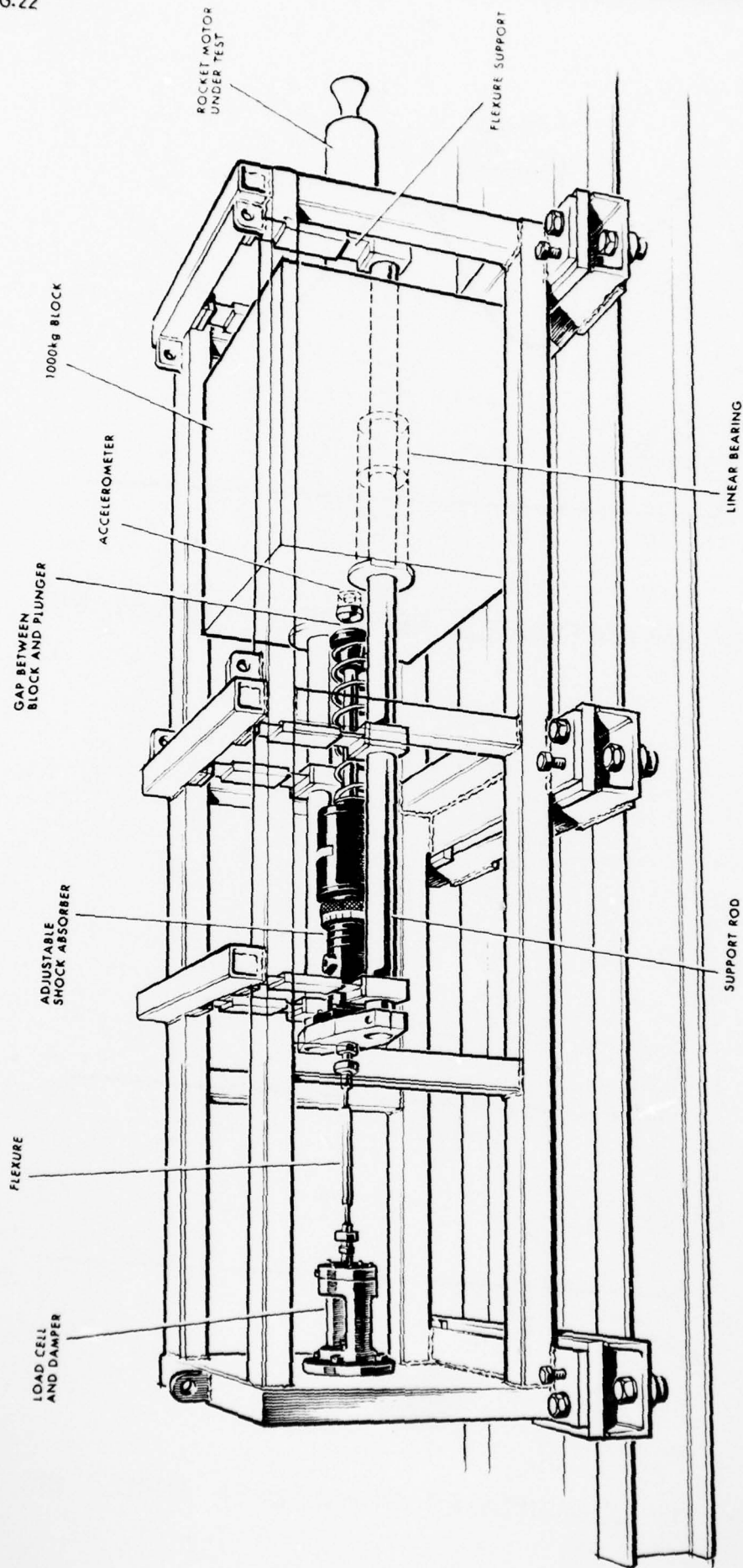


FIG. 22 BALLISTIC THRUST AND IMPULSE MEASURING DEVICE

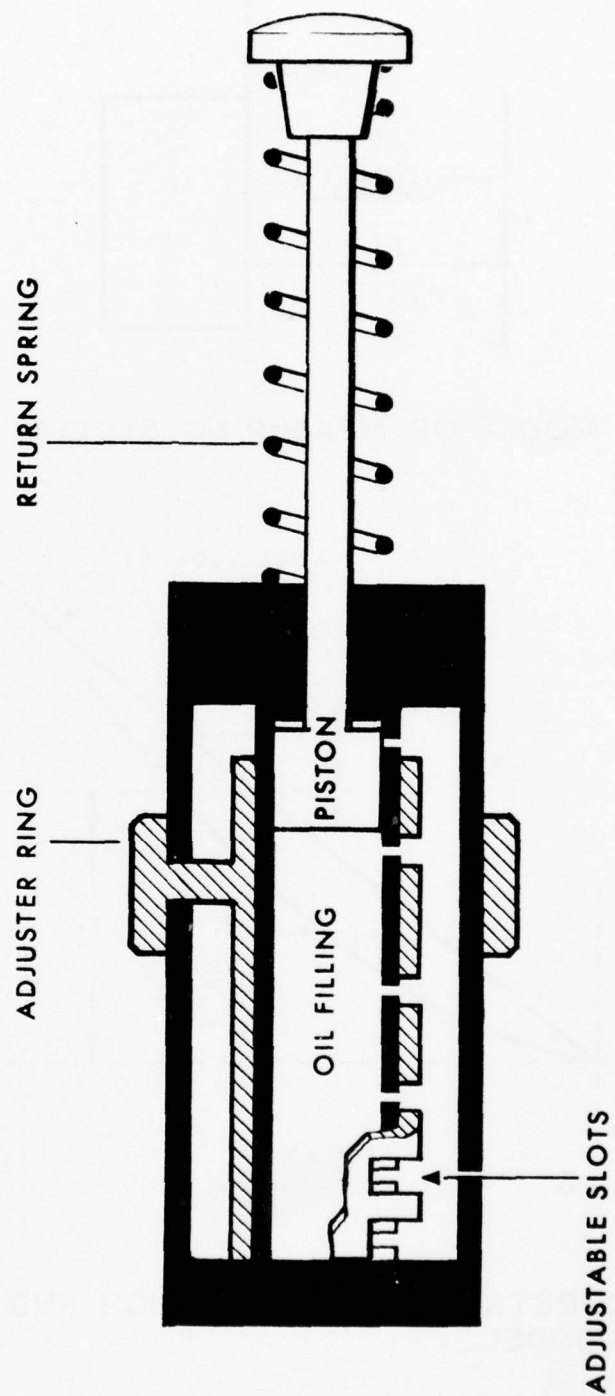


FIG. 23 DECELERATOR (DIAGRAMMATIC)

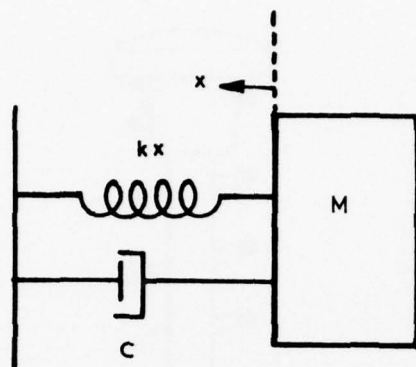


FIG.24 MODEL OF MEASURING SYSTEM

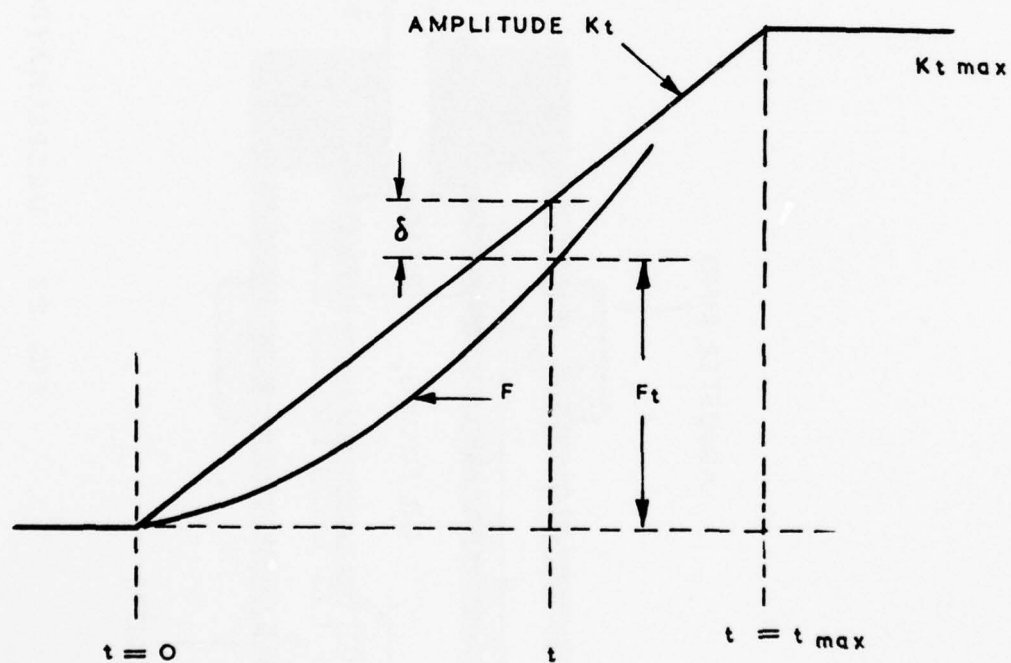


FIG.25 THEORETICAL INPUT FUNCTION AND RESPONSE OF MODEL

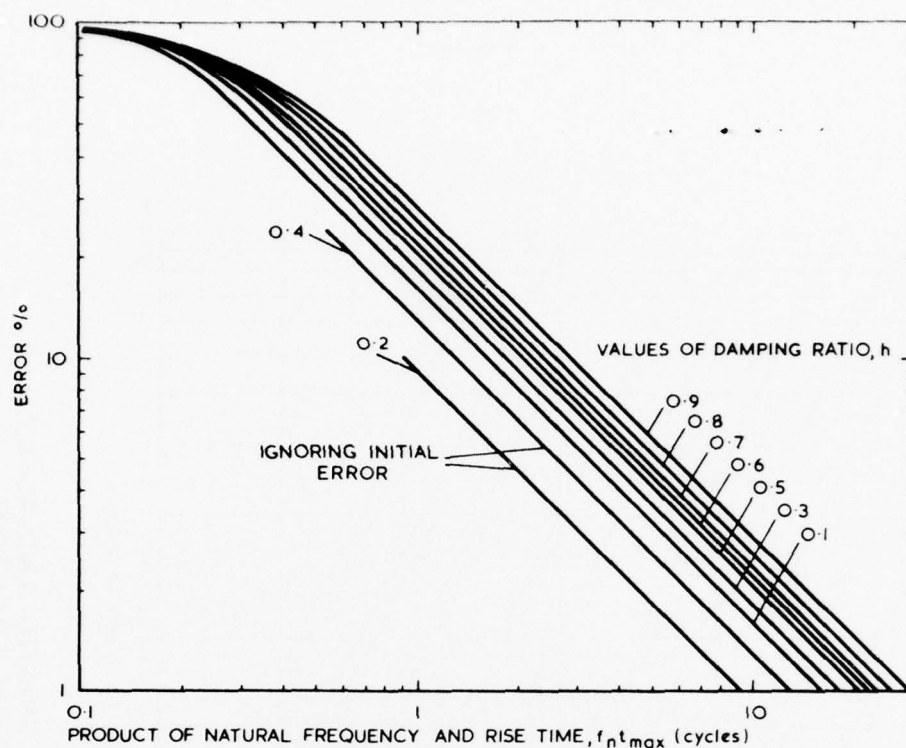


FIG. 26 MAXIMUM AMPLITUDE OR TIME ERROR AGAINST THE PRODUCT OF NATURAL FREQUENCY AND RISE TIME DURING RISE TIME

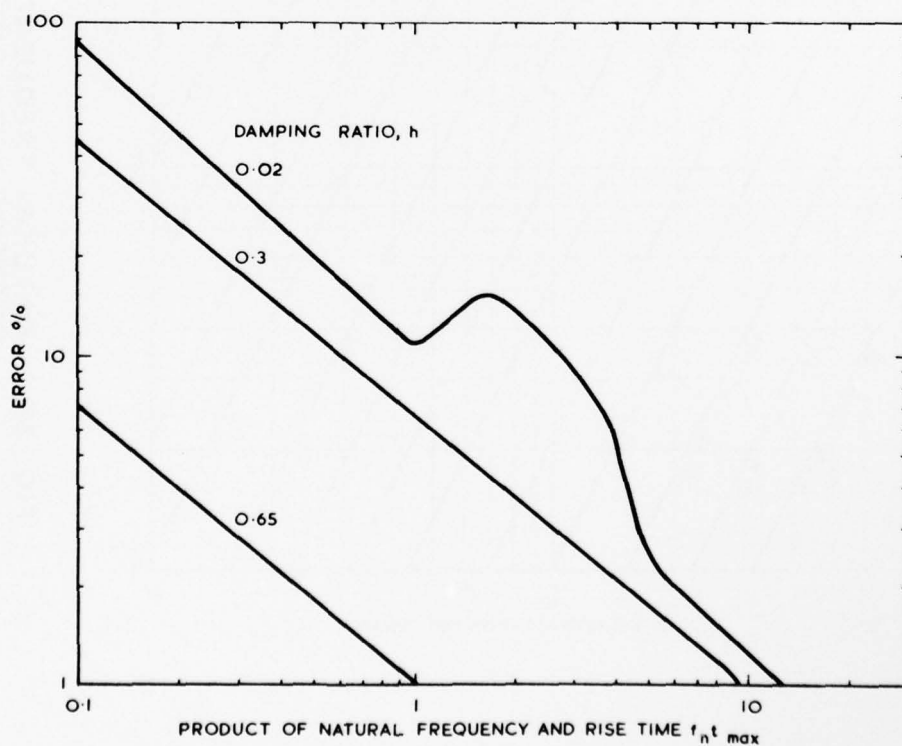


FIG. 27 MAXIMUM AMPLITUDE ERROR AGAINST THE PRODUCT OF NATURAL FREQUENCY AND RISE TIME AFTER TERMINATION OF RISE

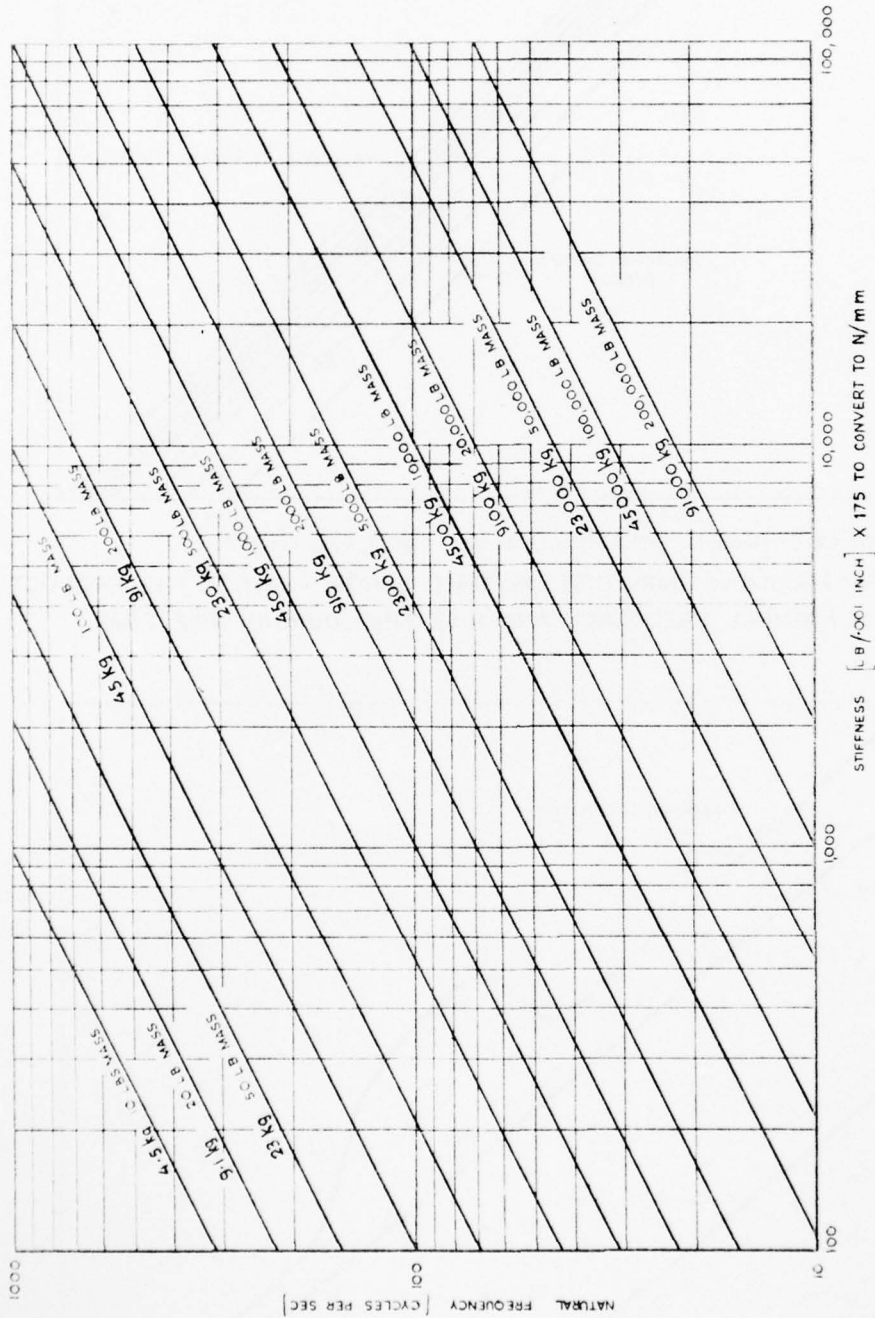


FIG. 28 NATURAL FREQUENCIES OF SPRING AND MASS SYSTEMS WITH ONE DEGREE OF FREEDOM

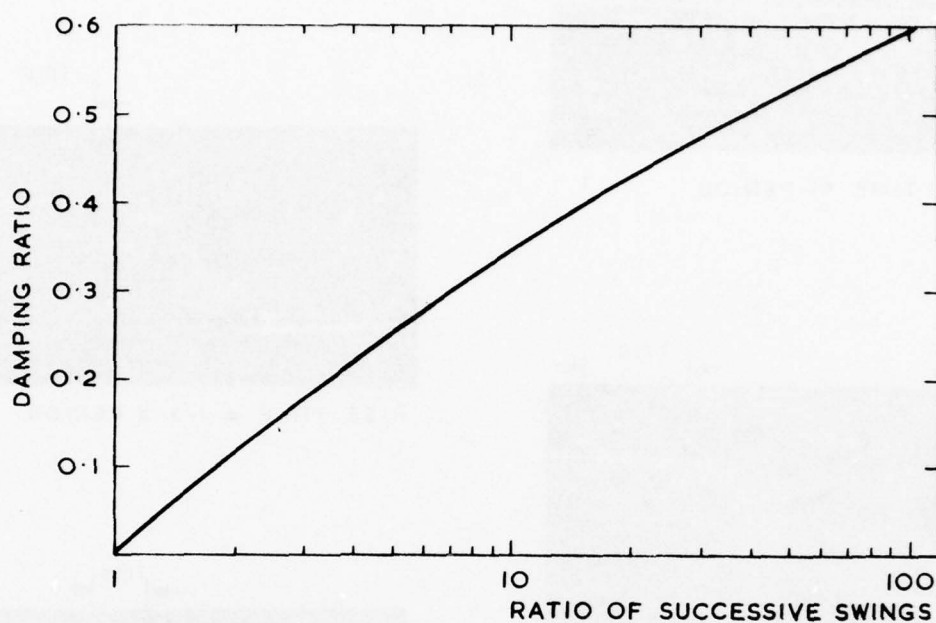


FIG. 29 DAMPING RATIO AGAINST RATIO OF AMPLITUDES OF SUCCESSIVE OSCILLATIONS

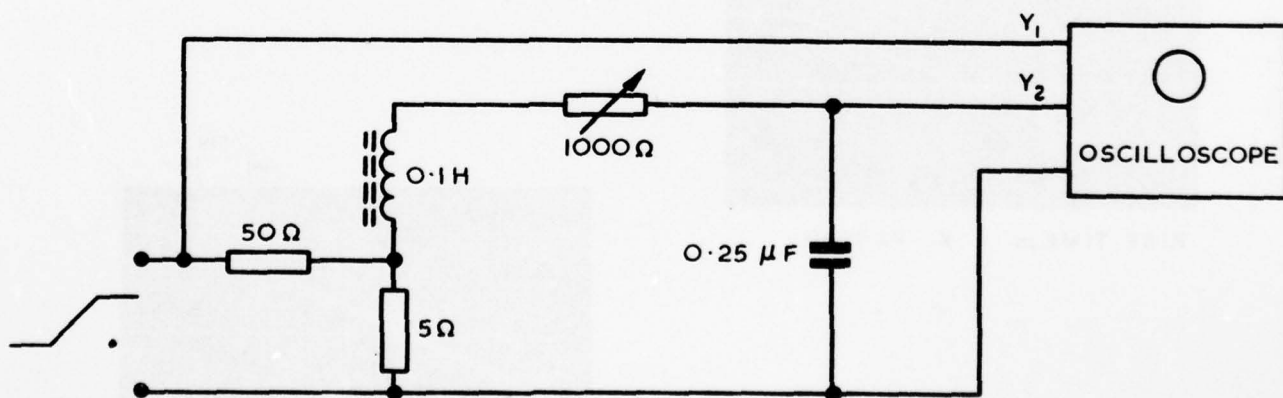
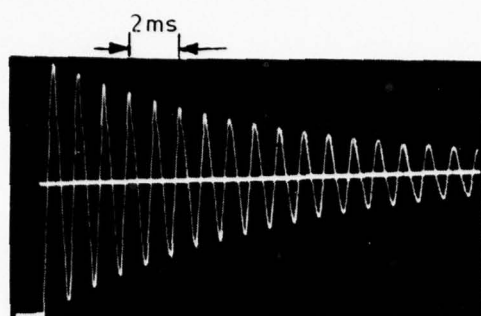
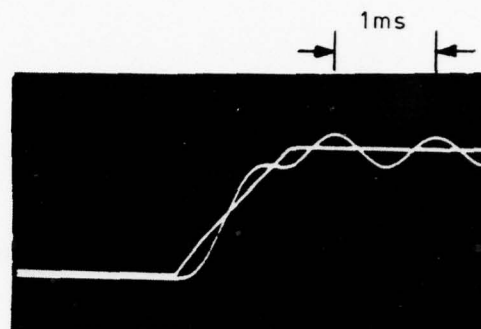


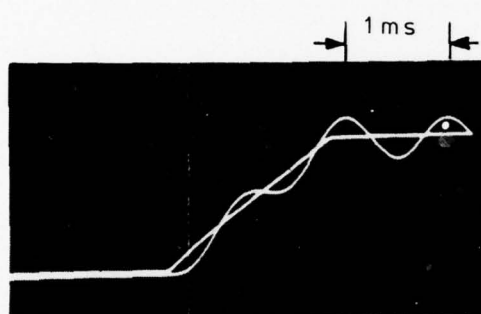
FIG. 30 ELECTRICAL ANALOGUE OF RESONANT SYSTEM



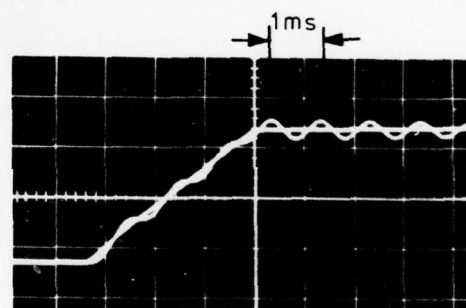
RISE TIME \ll PERIOD



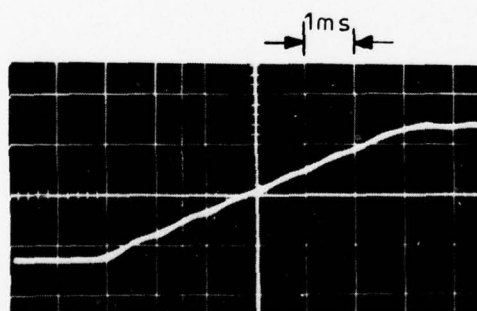
RISE TIME = 1.3 X PERIOD



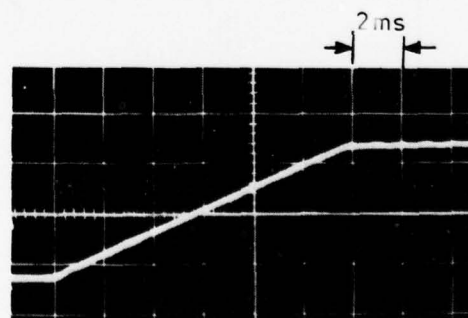
RISE TIME = 1.7 X PERIOD



RISE TIME = 3.3 X PERIOD

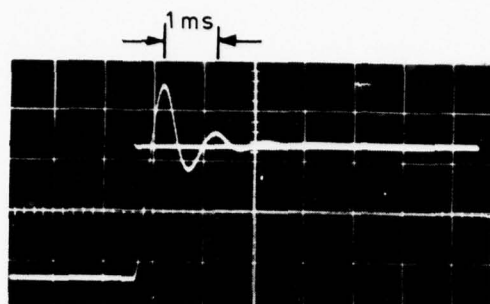


RISE TIME = 6 X PERIOD

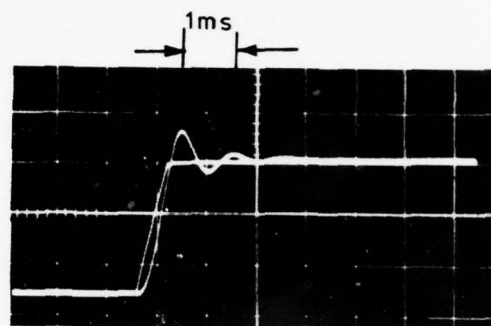


RISE TIME = 12 X PERIOD

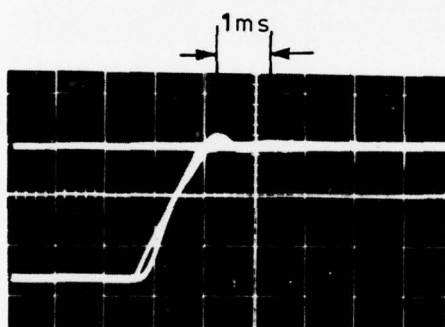
FIG. 31 RESPONSE OF MEASURING SYSTEM WITH DAMPING RATIO OF 0.02 AT VARIOUS RATIOS OF RISE TIME TO PERIOD OF MEASURING SYSTEM



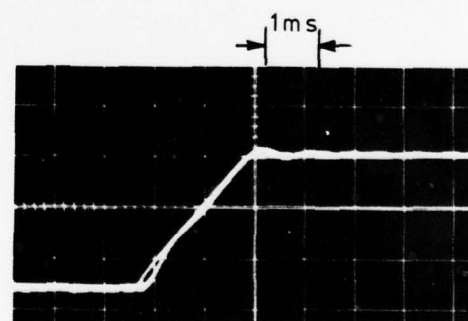
RISE TIME \ll PERIOD



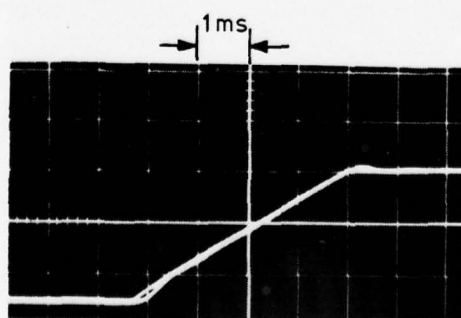
RISE TIME = $1/2$ PERIOD



RISE TIME = PERIOD

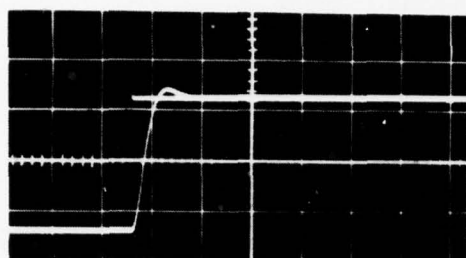


RISE TIME = 2 X PERIOD

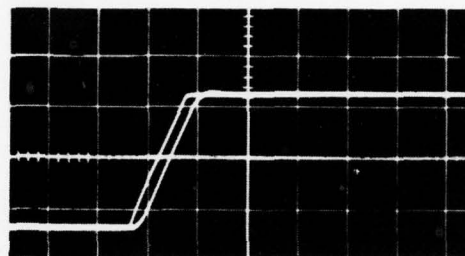


RISE TIME = 4 X PERIOD

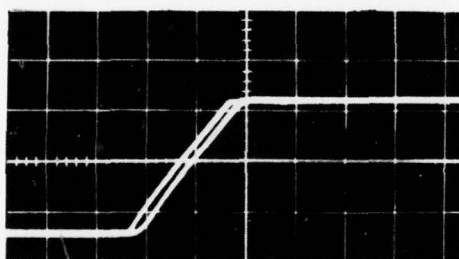
FIG. 32 RESPONSE OF MEASURING SYSTEM WITH DAMPING RATIO OF 0.3 AT VARIOUS RATIOS OF RISE TIME TO PERIOD OF MEASURING SYSTEM



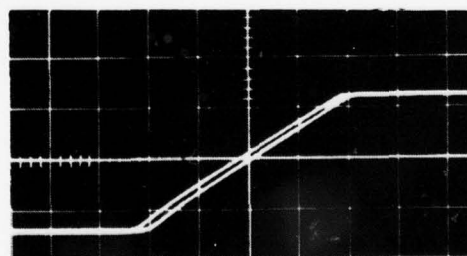
RISE TIME \ll PERIOD



RISE TIME = PERIOD



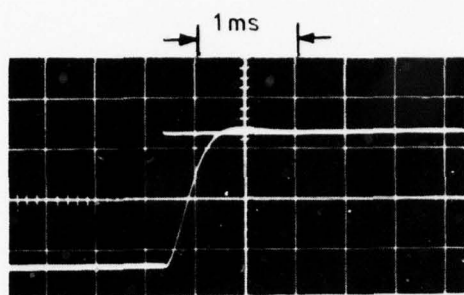
RISE TIME = 2 X PERIOD



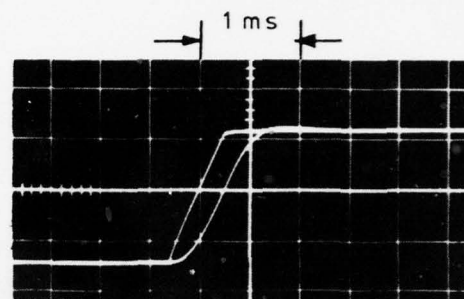
RISE TIME = 4 X PERIOD

ALL TIMING LINES AT 1m sec INTERVALS

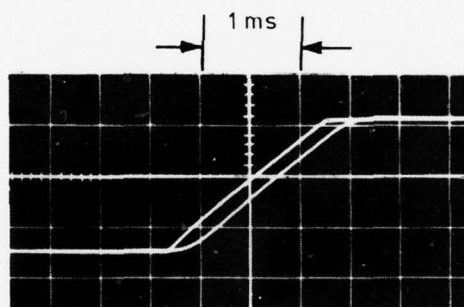
FIG.33 RESPONSE OF MEASURING SYSTEM WITH DAMPING RATIO OF 0.64 AT
VARIOUS RATIOS OF RISE TIME TO PERIOD OF MEASURING SYSTEM



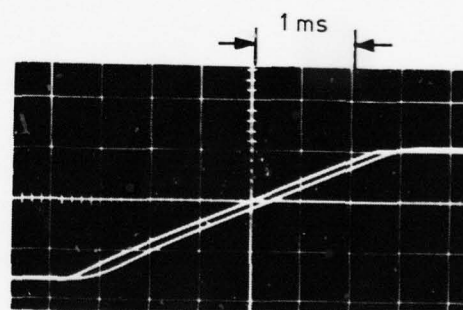
RISE TIME \ll PERIOD



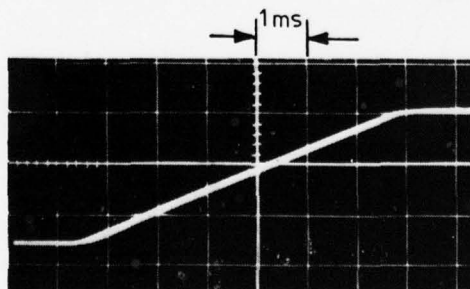
RISE TIME = $0.5 \times$ PERIOD



RISE TIME = $1.5 \times$ PERIOD



RISE TIME = $3 \times$ PERIOD



RISE TIME = $6 \times$ PERIOD

FIG.34 RESPONSE OF MEASURING SYSTEM WITH CRITICAL DAMPING AT VARIOUS RATIOS OF RISE TIME TO PERIOD OF MEASURING SYSTEM

AD-A059 700

PROPELLANTS EXPLOSIVES AND ROCKET MOTOR ESTABLISHMENT--ETC F/G 21/8
CURRENT TECHNIQUES FOR THRUST MEASUREMENT AT PERME WESTCOTT.(U)
FEB 78 D S DEAN

UNCLASSIFIED

PERME-TR-50

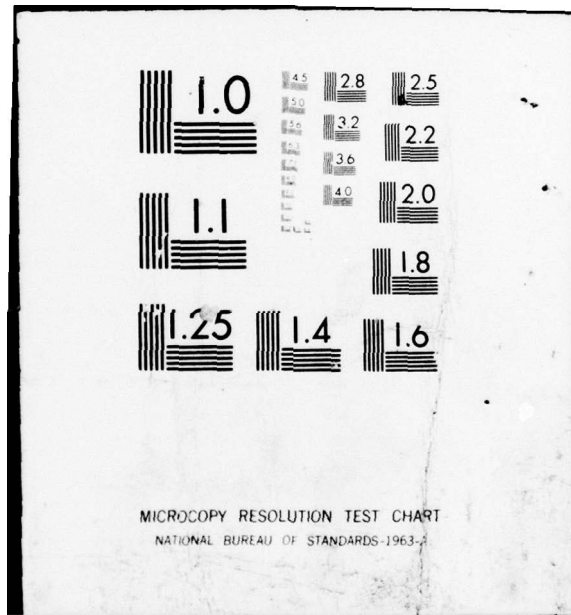
DRIC-BR-61445

NL

2 of 2
AD
A059700



END
DATE
FILMED
12-78
DDC



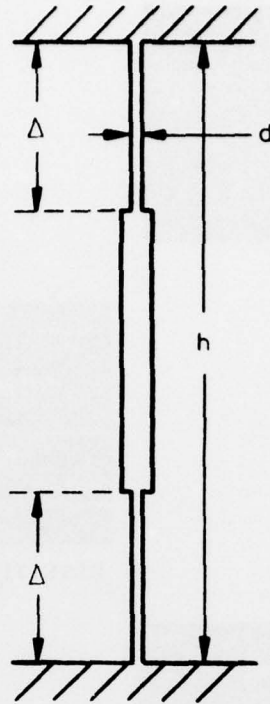


FIG.35

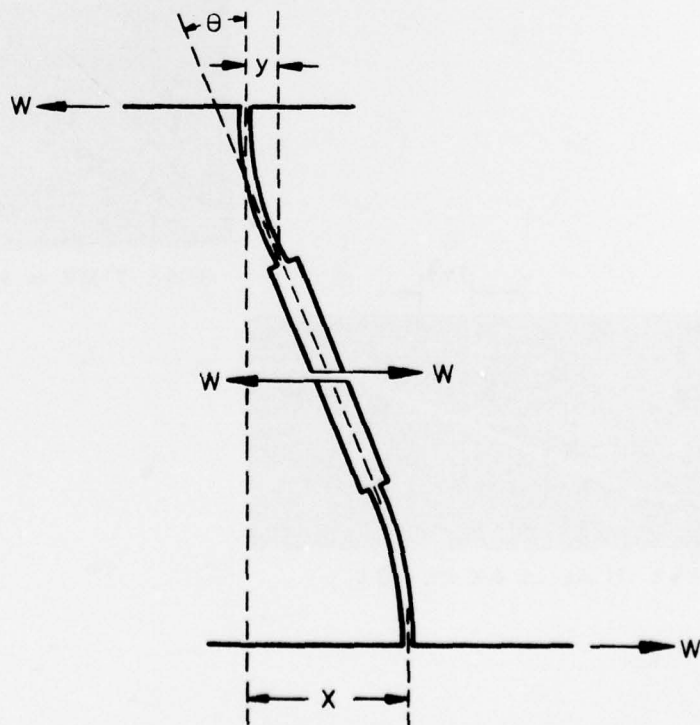


FIG. 36

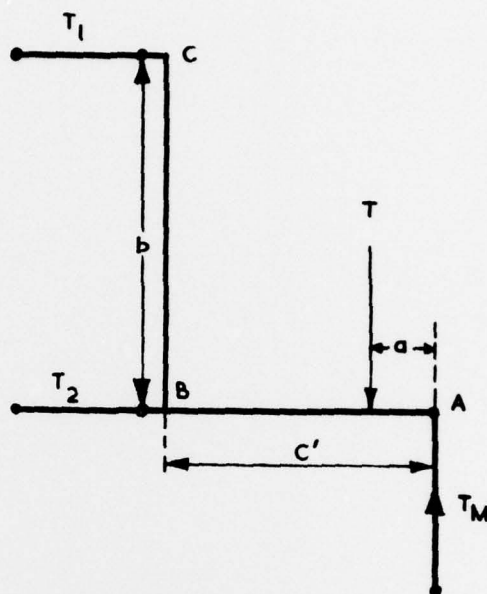


FIG. 37a STRUTS ALIGNED

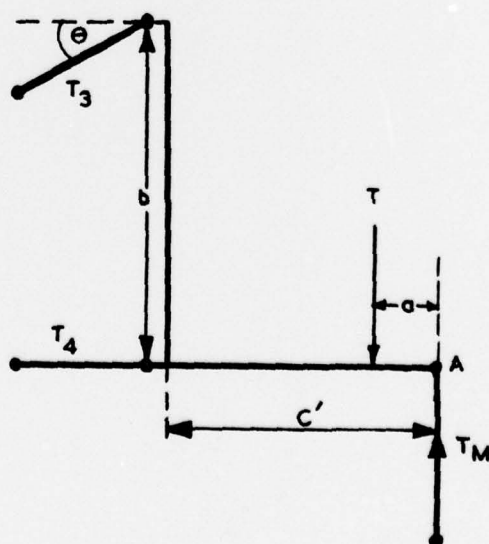


FIG. 37b UPPER STRUT MISALIGNED

DOCUMENT CONTROL SHEET
(Notes on completion overleaf)

Overall security classification of sheet **UNCLASSIFIED**

(As far as possible this sheet should contain only unclassified information. If it is necessary to enter classified information, the box concerned must be marked to indicate the classification eg (R), (C) or (S)).

1. DRIC Reference (if known)	2. Originator's Reference Technical Report No. 504	3. Agency Reference	4. Report Security Classification Unlimited
5. Originator's Code (if known)	6. Originator (Corporate Author) Name and Location Propellants, Explosives and Rocket Motor Establishment Westcott, Aylesbury, Bucks		
5a. Sponsoring Agency's Code (if known)	6a. Sponsoring Agency (Contract Authority) Name and Location		
7. Title Current techniques for thrust measurement at PERME Westcott			
7a. Title in Foreign Language (in the case of translations)			
7b. Presented at (for conference papers). Title, place and date of conference			
8. Author 1, Surname, initials Dean, D.S.	9a. Author 2	9b. Authors 3, 4...	10. Date pp ref 2.1978 97 1
11. Contract Number	12. Period	13. Project	14. Other References
15. Distribution statement			
<p>Descriptors (or keywords)</p> <p>Thrust measurement; Force; Impulse; Load cells; Signal conditioning; Data collection; Data analysis; Dynamic response</p> <p style="text-align: right;">continue on separate piece of paper if necessary</p>			
<p>Abstract</p> <p>Techniques are described for the measurement of axial thrust and thrust alignment of rocket motors. The dynamic response of systems is also considered and methods of evaluating errors derived. A ballistic technique for recording total impulse and thrust/time curves of motors with very short burning times is included.</p>			

ED
78